The oxygen sensor Prolyl hydroxylase domain 2 regulates the in vivo suppressive capacity of regulatory T cells

Yousra Ajouaou[1,2], Abdulkader Azouz[1,3], Anaelle Taquin[1,2], Sebastien Denanglaire[1,2], Hind Hussein[1,2], Mohammad Krayem[4,5], Fabienne Andris[1,2], Muriel Moser[1,2,], Stanislas Goriely[1,2,3] and Oberdan Leo[1,2*]

[1]U-CRI (ULB Center for Research in Immunology), Université Libre de Bruxelles (ULB), Gosselies, Belgium,
[2]Immunobiology laboratory, Université Libre de Bruxelles (ULB), Gosselies, Belgium,
[3]Institute for Medical Immunology, Université Libre de Bruxelles (ULB), Gosselies, Belgium,
[4]Department of Radiation Oncology, Institut Jules Bordet, Université Libre de Bruxelles, Brussels, Belgium,
[5]Laboratory of Clinical and Experimental Oncology (LOCE), Institut Jules Bordet, Université Libre de Bruxelles, Brussels, Belgium.

*Corresponding author: Oberdan Leo (Oberdan.Leo@ulb.be), Immunobiology laboratory, IBMM, Rue des Professeurs Jeener et Brachet 12, 6041 Gosselies (Belgium).

Abstract

The oxygen sensor PHD2 (prolyl hydroxylase domain 2) plays an important role in cell hypoxia adaptation by regulating the stability of HIF proteins (HIF1α and HIF2α) in numerous cell types including T lymphocytes. The role of oxygen sensor on immune cells, in particular on regulatory T cell (Treg) function, has not been fully elucidated. The purpose of our study was to evaluate the role of PHD2 in the regulation of Treg phenotype and function. We demonstrate herein that selective ablation of PHD2 expression in Treg (PHD2$^{\Delta Treg}$ mice) leads to a spontaneous systemic inflammatory syndrome, as evidenced by weight loss, development of a rectal prolapse, splenomegaly, shortening of the colon and elevated expression of IFN-γ in the mesenteric lymph nodes, intestine and spleen. PHD2 deficiency in Tregs led to an increased number of activated CD4 conventional T cells expressing a Th1-like effector phenotype. Concomitantly, the expression of innate-type cytokines such as *Il1b*, *Il12a*, *Il12b* and *Tnfa* was found to be elevated in peripheral (gut) tissues and spleen. PHD2$^{\Delta Treg}$ mice also displayed an enhanced sensitivity to DSS-induced colitis and to toxoplasmosis, suggesting that PHD2-deficient Tregs did not efficiently control inflammatory response in vivo, in particular those characterized by IFN-γ production. Further analysis revealed that Treg dysregulation was largely prevented in PHD2-HIF2α (PHD2-HIF2α$^{\Delta Treg}$ mice), but not in PHD2-HIF1α (PHD2-HIF1α$^{\Delta Treg}$ mice) double KOs, suggesting an important and possibly selective role of the PHD2-HIF2α axis in the control of Treg function. Finally, the transcriptomic analysis of PHD2-deficient Tregs identified the STAT1 pathway as a target of the PHD2-HIF2α axis in regulatory T cell phenotype and in vivo function.

Key words: Regulatory T cells/ Oxygen sensor/ Hypoxia inducible factor/ Inflammation

Introduction

$CD4^+$ regulatory T cells (Tregs), accounting for approximately 5-10% of total circulating $CD4^+$ T cells, represent a critical subset of T lymphocytes involved in immune homeostasis. Through a broad set of effector mechanisms, these cells contribute to immune tolerance to self-constituents and to mucosal antigens derived from the commensal microflora and food[1,2]. Tregs also participate in the resolution of inflammatory responses[3] and play an important role in maternal immunotolerance against the semi-allogeneic fetus[4]. While critical to maintain tissue integrity, excessive activation of Tregs impedes adequate immune responses to tumors and pathogens, suggesting a tight control of their suppressive activity and tissue localization[5–7]. Although uniformly characterized by the expression of the lineage-specific, Foxp3 transcription factor[1], regulatory T cells display a wide range of phenotypic and functional properties that allow them to migrate to specific sites and suppress a variety of immune reactions including inflammatory[8] and humoral responses[9]. Although diverse, the mechanisms whereby Tregs antagonize the activity of immune effectors are largely paracrine in nature[10]. Short-range suppressive mechanisms include competition for nutrients and/or growth factors (mostly cytokines), secretion of immunosuppressive factors and direct, contact-mediated, inactivation of antigen presenting cells[11]. These findings suggest that Tregs have to adapt to multiple lymphoid and non-lymphoid environments and suppress immune responses in a context and tissue-dependent fashion[12,13].

Oxygen represents an essential component of cellular bioenergetics and biochemistry. Because oxygen tension varies according to tissues and pathophysiological states[14], cells need to adapt to fluctuations in oxygen availability in order to maintain an adequate functional and metabolic status. Of note, low oxygen availability (hypoxia) plays a critical role in the pathophysiology of many immune disorders[15,16]. Inflammation, in particular, is thought to reduce oxygen availability to tissues by affecting microvascular form and function, and through the recruitment of highly oxygen consuming inflammatory cells producing NADPH oxidase-derived reactive oxygen species[17].

Immune cells patrolling through lymphoid and non-lymphoid tissues need therefore to readily adapt to varying oxygen concentration levels in order to exert their function[18], suggesting an important role for oxygen sensors in immune regulation. Several hypoxia-sensitive pathways are known to enable single cell survival in low oxygen settings. In particular, reduced oxygen levels are directly sensed by a family of oxygen-dependent prolyl hydroxylases (PHD encoded by *Egln gene,* comprising three members)[19], although other mechanisms mediated by oxygen-sensitive histone lysine demethylases (KDM) and the cysteamine dioxygenase/N-degron pathway have been recently uncovered[20]. Hypoxia-inducible factors (HIFs), a set of evolutionary conserved

transcriptional regulators, represent the best-described substrates of PHDs. These factors are heterodimers composed of a HIFα subunit whose stability is directly controlled by oxygen availability, and a constitutively expressed HIF1β subunit (also known as ARNT)[21]. Following the initial characterization of the first member of HIFα family (HIF1α), two additional members, HIF2α and HIF3α have been identified and shown to be similarly regulated by O_2 availability and to bind to HIF1β[22]. In normoxia, PHDs, whose affinity for oxygen is low and comparable to atmospheric concentrations, catalyze the prolyl-hydroxylation of HIFα subunits[23]. This post-translational modification allows recognition and ubiquitination of HIFα subunits by the E3 ubiquitin ligase Von Hippel-Lindau protein (pVHL) and subsequent degradation by the proteasome[24]. In hypoxia, non-hydroxylated alpha subunits escape degradation, and translocate to the nucleus where they bind to constitutively expressed and stable beta subunits to constitute an active heterodimer able to regulate gene expression. This process promotes transcriptional regulation of numerous genes ultimately leading to increased oxygen supply (such as angiogenesis) and promotion of anaerobic metabolism[25].

Multiple levels of complexity of this major regulatory axis have been recently uncovered. As previously suggested, the presence of several members of the PHD and HIF families suggests specialized functions of PHD-HIF pairs during ontogeny and in selected tissues[26]. In particular, while HIF1α appears as ubiquitously expressed in all metazoans, HIF2α represents a late acquisition of vertebrates, displaying a more restricted tissue expression pattern[27]. Although these factors bind to similar sequence motifs (hypoxia response elements or HREs) and regulate the expression of a shared set of genes, both HIF1α and HIF2α specific gene targets have been identified in multiple tissues[25,28,29]. Further complexity in this pathway has been provided by the identification of additional, non-HIF-related, PHD substrates, suggesting a role of proline hydroxylation in other settings requiring oxygen-dependent regulation[30–37].

Hypoxia plays a dual role in inflammation and in the regulation of immune responses. In most settings, hypoxia promotes inflammation, while in some instances, such as in tumor sites, low oxygen levels generally cause unresponsiveness of immune effectors, thus favoring tumor growth. The often-opposing effects displayed by HIF activation on the activity of immune cells equally match this complexity[38]. Previous work has indeed highlighted the important role of the PHD-HIF axis in regulating both innate and adaptive immune effectors[26]. The role of HIF1α in regulating T cell activity has been described in many studies, and mainly linked to the capacity of this hypoxia-induced transcription factor to promote glycolysis (for a review see McGettrick & O'Neill[39]). Accordingly, HIF1α expression favors the development of highly glycolytic inflammatory Th17 cells, while inhibiting the development of Tregs which rely mostly on aerobic metabolism[40]. HIF1α also plays a direct role in Th17 development, through the transcriptional activation of *Rorc*[41]. The role of HIF1α in Th1 development appears as more complex, and context-

dependent. Hypoxia decreases IFN-γ production of Th1-like cells in a HIF1α dependent fashion[42], while sustained expression of this transcription factor in normoxia (as observed in mice lacking PHDs expression[43]) leads to an increase in IFN-γ secreting $CD4^+$ T cells. Of note, expression of HIF1α can be upregulated in normoxia both by TCR[44] and cytokine-initiated signals[41], confirming that HIF1α may play a role in Th1 cells development both in hypoxia and normoxia.

The role of hypoxia-induced factors in Treg development and function is presently not fully elucidated. As previously discussed, HIF1α-deficiency improves Treg cell development, possibly a consequence of the limited requirement for glycolysis of this cell subset[40]. However, hypoxia promotes Foxp3 expression in a HIF1α dependent fashion[45] (and expression of HIF1α is required for adequate regulatory T cell function[46]). Similarly, a recent report has identified HIF2α as an important mediator of Treg function in vivo, further stressing the important role of these hypoxia-induced factors in the control of in vivo inflammatory manifestations[47]. In agreement with these conclusions, PHDs proteins have also been shown to play a role in the differentiation of peripheral (but not thymic-derived) Tregs[43]. Expression of these proteins appears to redundantly regulate Th1 vs iTreg development, mostly by limiting the accumulation of HIF1α. In contrast to this study, a recent publication has highlighted a selective role of the PHD2 isoform in the regulation of Treg function[48]. ShRNA mediated knockdown of PHD2 expression in Foxp3-expressing cells (PHD2-KD Tregs) led to a systemic inflammatory syndrome characterized by mononuclear cell infiltration in several organs. PHD2-KD Tregs displayed reduced suppressive capacities both in vitro and in vivo, suggesting an important and intrinsic role of PHD2 in this cell subset. Of interest, loss of HIF2α expression reversed the phenotype of these mice bearing PHD2-KD Tregs, suggesting an important role of the PHD2-HIF2α axis in regulating Treg function.

To better delineate the role of PHD2, HIF1α and HIF2α in the regulation of Treg development and function, we have generated a set of conditional mouse strains lacking expression of these hypoxia responsive proteins in $Foxp3^+$ cells. Using these tools, we confirm herein that mice in which expression of PHD2 is selectively inactivated in regulatory T cells display a spontaneous inflammatory syndrome characterized by altered immune homeostasis at the steady-state and high sensitivity to Th1-type inflammatory diseases. This proinflammatory phenotype was accentuated by the concomitant loss of PHD2 and HIF1α, but almost completely alleviated in mice dually deficient for PHD2 and HIF2α. Transcriptome analysis confirmed a marginal role for HIF1α-dependent enhanced glycolysis in the regulation of Treg function and allowed us to identify STAT1 as a potential target of the PHD2-HIF2α axis in maintaining immune homeostasis and preventing excessive Th1-mediated inflammation.

Results

Deletion of PHD2 in Tregs leads to a systemic, type-1-like, inflammatory syndrome associated to altered Treg numbers and phenotype.

Based on the predominance of *Egln1* (PHD2) expression in Tregs over other members of the prolyl hydroxylases family, we generated a mouse strain lacking PHD2 expression in Tregs (identified as PHD2$^{\Delta Treg}$) (**Figure 1 and Figure 1-figure supplement 1**), as described in the Methods section. These mice displayed a strongly reduced expression of *Egln1* mRNA in Tregs, while retaining control level expression of this enzyme in other, non-Treg spleen and peripheral lymph node cells (**Figure 1-figure supplement 1**). Upregulation of GLUT1 expression, a well-known target of HIF1α, was also only found in Foxp3-expressing cells in these mice, further supporting the selective depletion of PHD2 in Tregs vs T convs (**Figure 1-figure supplement 1**). While fertile and viable, over 70% of these mice developed a spontaneous inflammatory syndrome, characterized by weight loss, episodes of anal prolapse, reduced colon length, splenomegaly and hemorrhagic abdomen (**Figure 1a-e**). This last feature is most likely due to an increased blood hematocrit (with enhanced numbers of circulating red blood cells) associated to an elevation in vascular permeability, as shown in **Figure 1-figure supplement 2**. Although the frequency of CD4^{+} and CD8^{+} conventional T lymphocytes (see **Figure 1-figure supplement 3** for gating strategy) in several lymphoid organs were not significantly altered in PHD2$^{\Delta Treg}$ mice (**Figure 1f**), the total number of CD4^{+} cells was increased in the peripheral lymphoid organs of these mice (**Figure 1-figure supplement 4**). Moreover, these lymphocytes displayed clear signs of spontaneous activation, as evidenced by the significant increase in the expression of markers (i.e CD44) associated to an effector-like phenotype (**Figure 1g, h**). Confirming these findings, intracellular staining of short-term stimulated T cells (using pharmacological agents bypassing TCR signaling) revealed an increased capacity of conventional T cells from PHD2$^{\Delta Treg}$ mice to produce IFN-γ, while retaining control-like production of IL-17 (**Figure 1i**). The ex-vivo evaluation of mRNA abundance in whole, unfractionated, mLNs similarly showed a significantly elevated expression of type 1-associated adaptive and innate cytokines including *Ifng*, *Il1b,* both *Il12* subunits and *Tnfa* (**Figure 1j**). Overall, these observations point to the establishment of a Th1-like, pro-inflammatory environment in mice possessing PHD2-deficient Tregs.

Much to our surprise, flow cytometric analysis of lymphoid organs from naive animals revealed an increased frequency of Treg cells in the spleen, lymph nodes and lamina propria of PHD2$^{\Delta Treg}$ mice, when compared to control animals (**Figure 2a**). To evaluate the possible influence of PHD2 deletion on Treg development, thymic cell suspensions were analyzed for the expression of early Treg markers including Foxp3, CD25 and

CD24[49]. Recent studies have revealed that mature Foxp3^{high} CD25^{+} Tregs can differentiate from two distinct thymic precursors identified as respectively CD25^{+} Foxp3^{-} and CD25^{-} Foxp3^{low} precursor Tregs (pre-Tregs). Analysis of thymic cell suspensions revealed an accumulation of the Foxp3^{low} pre-Tregs and a reduction in the number of mature Tregs in PHD2-deficient, Foxp3-expressing cells, suggesting an early role for PHD2 in the generation of thymic-derived Tregs (**Figure 2b, c**). Accordingly, PHD2-deficient, Foxp3-expressing cells retained higher expression of CD24 (**Figure 2d**), a marker associated to a thymic immature state[49], further confirming a putative role for PHD2 in the development of thymic-derived Tregs. No difference in the relative frequency of Treg subsets identified by the co-expression of Foxp3 with either naive and memory markers (**Figure 2e**) or with master transcription factors T-bet, GATA3 or RORγt (**Figure 2f**) was noted in these mice. The phenotype of splenic, PHD2-deficient Tregs was however significantly altered, showing a slight, but statistically significant reduction in the expression of Foxp3 (**Figure 2g**), accompanied by reduced expression of the CD25, ICOS, and CD44 markers and enhanced expression of PD-1 (**Figure 2h**). Of note, neither CTLA-4 (**Figure 2h**) nor *Il10* (**Figure 2i**) expression was altered in PHD2-deficient Tregs. To evaluate the functional consequences of PHD2-deletion on peripheral Treg development, we generated Tregs from naive, conventional T cells using a well-established in vitro protocol. In keeping with in vivo observations, culture of CD4^{+} T conv from PHD2$^{\Delta Treg}$ mice led to a consistently higher yield of Foxp3-expressing cells when activated in the presence of Treg-inducing cytokines (**Figure 2j, k**). In contrast to their in vivo counterparts, these induced Tregs displayed control level expression of Foxp3 (**Figure 2l**).

To evaluate whether the altered phenotype of PHD2-deficient Tregs was a cell-autonomous phenomenon, heterozygous *Foxp3*$^{cre/+}$ *Egln1*$^{fl/fl}$ mice in which both PHD2-sufficient (YFP-negative) and PHD2-deficient (YFP-positive) Tregs co-exist were examined (**Figure 3**). These mice did not display any sign of inflammation or hematological dysfunction and were morphologically (cf weight, colon length and spleen size) indistinguishable from Foxp3^{cre} or Foxp3$^{cre/+}$ mice (this latter strain displaying the expected 1:1 ratio of YFP-pos:YFP-neg cells). Surprisingly, WT Tregs outcompeted PHD2-deficient Tregs in all compartments examined in *Foxp3*$^{cre/+}$ *Egln1*$^{fl/fl}$ mice (i.e. thymus, spleen, and peripheral lymph nodes, **Figure 3a**). A similar trend was observed following the transfer of an equal mix of WT and PHD2-deficient Tregs in *Rag2*-deficient mice (data not shown), strongly suggesting that PHD2 expression plays a role in Treg fitness and survival in the periphery. As previously shown in **Figure 2**, PHD2-deficient Tregs expressed lower levels of Foxp3, CD25 and CD44, indicative of an intrinsic role of PHD2 in regulating Treg phenotype (**Figure 3b-e**). However, expression of CTLA-4 was not altered in PHD2-deficient Tregs (**Figure 3b, f**). Whether the altered fitness / capacity to repopulate the periphery of PHD2-deficient Tregs is due to reduced expression of CD25 remains to be established.

In vivo reduced suppressive function of PHD2-deficient Tregs.

To evaluate the suppressive capacity of PHD2-deficient Tregs cells, ex-vivo purified CD45.2 expressing Tregs from control and PHD2$^{\Delta Treg}$ mice were adoptively co-transferred into syngeneic Rag-deficient mice with CFSE-labelled, CD45.1-expressing CD4^{+} naive T lymphocytes (**Figure 4a**). In the absence of Tregs, transferred naive cells rapidly divided and acquired an effector-like phenotype, a well-established consequence of homeostatic proliferation in a lymphopenic environment (**Figure 4b**). Addition of WT Tregs in the inoculum led to a significant reduction of conventional T cell proliferation and phenotype switch, while PHD2-deficient Tregs appeared functionally impaired in this assay (**Figure 4b-d**). Lack of suppressive activity of these Tregs was not a consequence of reduced viability and/or in vivo survival, as shown by the normal recovery rate of both Treg-populations at the time of assay read-out (**Figure 4e**). In contrast, when tested in vitro, PHD2-deficient Tregs consistently displayed a fully functional suppressive activity (**Figure 4f, g**).

Increased susceptibility of PHD2$^{\Delta Treg}$ mice to type-1 experimental inflammation

A series of experimental acute and chronic inflammatory models were employed to further evaluate the capacity of PHD2$^{\Delta Treg}$ mice to sustain an in vivo inflammatory challenge. We first exposed mice to a chemical-induced colitis protocol. This assay revealed an increased sensitivity of PHD2$^{\Delta Treg}$ mice to most DSS-induced inflammatory manifestations, including weight loss (**Figure 5a**), survival (**Figure 5b**), clinical score (**Figure 5c**) and colon length (**Figure 5d)**. No difference was noted however in crypt morphology induced by DSS in both mouse strains (**Figure 5e**). Similar observations were made when mice were acutely infected with *Toxoplasma gondii*, a model of infection-induced pathology (**Figure 5f**). Infected PHD2$^{\Delta Treg}$ mice displayed increased weight loss (**Figure 5g**), reduced colon length (**Figure 5h**) and increased frequency of activated cells characterized by an effector-like phenotype (**Figure 5i**) and IFN-γ secretion capacity (**Figure 5j**). Infected PHD2$^{\Delta Treg}$ mice also displayed a decrease in Treg T-bet^{+} frequency, a population known to control Th1 inflammation during toxoplasmosis[50] (**Figure 5k**). Overall, PHD2$^{\Delta Treg}$ mice displayed an uncontrolled expansion of Th1-like cells following experimental toxoplasmosis. In contrast, both PHD2-deficient and sufficient mouse strains were equally sensitive to enteritis induced upon injection of anti-CD3 antibodies (**Figure 5-figure supplement 1**), a model known to induce the predominant expansion of Th17-like, inflammatory effectors in vivo[51]. The role of uncontrolled IFN-γ secretion in mediating the pro-inflammatory status of this mouse strain was further confirmed by the observation that ubiquitous loss of *Ifng* gene expression largely reversed the phenotypical and cellular altered status of PHD2$^{\Delta Treg}$ mice (**Figure 5-figure supplement 2**).

Concomitant loss of HIF2α, but not HIF1α, expression partially corrects the pro-inflammatory phenotype of PHD2$^{\Delta Treg}$ mice.

Based on the notion that HIF1α and HIF2α represent well-described targets of PHD2, we established a series of conditional KOs mouse strains to identify the molecular pathway responsible for the decreased functional activity of PHD2-deficient Tregs at steady state (**Figure 6**) (see **Figure 6-figure supplement 1** for strain validation). Treg-selective deletion of HIF1α and HIF2α expression alone did not significantly alter colon length (used as a proxy for spontaneous inflammation) nor general T cell immune homeostasis (**Figure 6-figure supplement 1**). The same observation was made for double HIF1α and HIF2α KOs (data not shown). In marked contrast, combined deletion of PHD2 and HIF2α reversed some of the inflammatory symptoms observed in PHD2$^{\Delta Treg}$ mice, such as splenomegaly, colon length (**Figure 6a, b**) and hematocrit counts (**Figure 1-figure supplement 2**). Treg specific, PHD2-HIF1α double KOs were virtually indistinguishable from PHD2$^{\Delta Treg}$ according to these morphological criteria. Noteworthy however, Treg-specific PHD2-HIF1α double KOs mice were born at sub-mendelian ratios, and displayed a marked weight loss during adult life and reduced viability, indicative of a more pronounced pro-inflammatory status (data not shown). This mouse strain also displayed a tendency toward increased expansion of Th1-like cells in peripheral lymph nodes (**Figure 6e**). PHD2-HIF1α-HIF2α triple KOs and PHD2-HIF2α double KOs displayed a similar phenotype, establishing a predominant role for HIF2α over HIF1α in mediating the effects of PHD2 on the capacity of Treg to regulate immune homeostasis at rest. Similarly, lack of HIF2α expression largely reversed the altered phenotype of conventional T cells induced by loss of Treg-associated PHD2 expression. Indeed, cells from double (PHD2-HIF2α) and triple (PHD2-HIF1α-HIF2α) Treg specific KOs displayed a near normal phenotype (based on CD62L and CD44 expression) and propensity to secrete IFN-γ (**Figure 6c-e**). Finally, loss of Treg-associated expression of HIF2α also reversed the expansion of Treg numbers (**Figure 6f**) and restored Foxp3 protein expression to near-control levels (**Figure 6g**).

Transcriptomic analysis identifies cell survival, response to chemokines and STAT1-mediated signaling as target pathways of the PHD2-HIF2α axis in Tregs.

Collectively, the previous observations suggest that the PHD2-HIF2α regulatory axis confers to Tregs the capacity to control the spontaneous, type-1 like, activity of conventional T cells. To identify PHD2-dependent signaling pathways operating in Tregs, splenic Foxp3-expressing cells were purified from all mouse strains described in this manuscript and their transcriptome analyzed following bulk RNA-seq. A set of 532 genes were found differentially expressed between WT and PHD2-deficient Tregs (**Figure 7**) (a summary-list of upregulated and downregulated pathways in PHD2$^{\Delta Treg}$ mice vs Foxp3^{cre} mice is provided in **Figure 7-figure supplement 1**). Differential gene

expression analysis between all mouse strains studied identified 1868 genes differentially expressed between groups. An unsupervised clustering of the differentially expressed genes led to the identification of 20 clusters, as shown in **Figure 7a**. To identify gene clusters that were specifically involved in the immune homeostatic control of naive mice, the RNA-seq data were filtered and grouped by k-mean clustering. We next searched for sets of genes whose expression best correlated with an arbitrary inflammatory index, established based on previously described findings (mostly colon length, splenomegaly and spontaneous conventional T cell activation status) and summarized in **Figure 7b**. In particular, while concomitant deletion of HIF1α expression worsened the inflammatory status of PHD2$^{\Delta Treg}$ mice, loss of HIF2α expression mitigated most inflammatory-related parameters at rest. We therefore clustered genes according to a "gradient of disease severity" and grouped them in sets of gene whose expression decreased (cluster 10, **Figure 7c**) or increased (cluster 11, **Figure 7d**) accordingly. Gene ontology analysis of these clustered gene sets revealed the following. Reduced expression of cell death-related and gain of survival-associated gene expression correlated with the increased frequency of Tregs in the corresponding mouse strains (**Figure 7c, d**). Not surprisingly, the expression of genes associated with anti-inflammatory responses was gradually lost according to the same severity gradient. Finally, genes, associated with T cell migration, including several chemokine receptors, also displayed an ordered loss of expression along the same gradient (**Figure 7c**). For comparison purposes, genes whose expression was restored to control levels upon combined deletion of PHD2 and HIF1α were also examined. As expected from previously published findings, these HIF1α-dependent biological pathways included glycolysis and angiogenesis (**Figure 7e**).

Ingenuity Pathway Analysis (IPA) was performed in order to identify possible upstream regulators affecting expression of downstream genes identified in clusters 10 and 11. This analysis led to the identification of STAT1 as a putative upstream transcription factor regulating the expression of a set of genes whose expression was altered in PHD2-deficient Tregs (**Figure 8a**). Since *Stat1* mRNA expression was not altered by PHD2 invalidation (as revealed by RNA-Seq analysis), we tested the capacity of STAT1 to undergo phosphorylation in response to IFN-γ. This set of experiments led to the identification of a defective, accumulation of phopho-STAT1 in PHD2-deficient Tregs (**Figure 8b, c**), while the levels of total STAT1 protein appeared unaffected (**Figure 8d**). Noteworthy, concomitant deletion of HIF2α restored a near control response to IFN-γ in PHD2 deficient Tregs (**Figure 8b-d**). In keeping with the observed pro-inflammatory phenotype associated with these mouse strains, conventional T cells from PHD2$^{\Delta Treg}$ mice displayed an augmented response to IFN-γ (as judged by pSTAT1 accumulation), partially reversed in mice bearing Tregs lacking both PHD2 and HIF2α expression (**Figure 8b, left panel**). Finally, the proportion of Tregs expressing CXCR3, a well described STAT1-dependent chemokine receptor[52] was reduced in a HIF2α-

dependent manner in PHD2-deficient Tregs (**Figure 8e**), further strengthening the conclusion that PHD2 expression controls the response of Tregs to IFN-γ.

Discussion

The present study highlights the important role of the prolyl-hydroxylase PHD2 in the regulation of Treg development and function. Deletion of PHD2 in developing, Tregs led to the accumulation of the subset of Treg precursor characterized by low expression of Foxp3, at the expenses of the mature, $Foxp3^{+}CD25^{+}$ Treg population (**Figure 2c**). PHD2-deficient Tregs were nevertheless found in increased numbers in vivo at steady state (**Figure 2a**), albeit with an altered phenotype. In particular, the expression of molecules known to be associated with optimal suppressive activity (such as Foxp3, ICOS and CD25)[1,53,54] was marginally decreased, while expression of PD-1, a marker associated with altered functional activity of many immune cells including Tregs[55,56] was augmented. Of note, other molecules known to play an important role in Treg function were expressed at optimal levels (cf CTLA4 and IL-10).

Although we have not specifically addressed the role of PHD2 in thymic vs peripherally induced Tregs, it is noteworthy that lack of PHD2 expression altered Treg thymic development, without any major effect on the generation of iTreg in vitro, suggesting a more pronounced role of PHD2 on thymic vs peripherally generated Tregs, although this conclusion should be strengthened by additional studies.

Mice selectively lacking PHD2-expression in Treg displayed a proinflammatory phenotype (with early manifestations of gastrointestinal tract inflammation), associated to an elevated hematocrit, enhanced vascular permeability and an altered homeostatic profile of splenic conventional T cells. In marked contrast to WT Tregs, PHD2-deficient Tregs express relatively high levels of *Vegfa* transcripts (as established from RNAseq analysis), a factor known to both increase vascular permeability[57], and induce erythropoietin (Epo) production from perivascular stromal cells in several organs[58]. Alternatively, since expression of the YFP-Cre allele was found in a minor, proportion of CD45-negative cells in all organs examined (see **Figure 8-figure supplement 1**). PHD2-deletion could result in elevated expression of Epo from a non-hematopoietic source. In any event, analysis of several organs (including spleen, liver and kidney) from $PHD2^{\Delta Treg}$ mice failed to reveal any increase in *Epo* mRNA accumulation (our own unpublished observations), and further studies will therefore be required to identify the mechanism underlying the observed hematological alterations in $PHD2^{\Delta Treg}$ mice. Several observations however strongly indicate that the major, proinflammatory phenotype observed in these mice were due to the specific impairment in Treg function consequent to the loss of PHD2 activity. Despite previous reports describing the stochastic activity of the *Foxp3*-Cre-YFP allele in non-Tregs leading to the recombination

of some, but not all alleles[59], we consistently found a control-level expression of PHD2 in all conventional T cell subset tested (**Figure 1-figure supplement 1**). Secondly, co-transfer of highly purified Tregs with WT naive $CD4^+$ conventional target cells clearly demonstrated an intrinsic role of PHD2 in regulating Treg function. Finally, and this will be discussed further below, mice bearing double PHD2-HIF2α-deficient Tregs recover a near-control phenotype, further excluding a major influence of the genetic background on the observed phenotype. Our observations confirm and further extends observations from a study published during completion of our work[48], indicating a specific, non-redundant role for PHD2 in controlling Treg activity in vivo.

Based on the notion that hypoxia-induced factors represent major substrates of PHD2, we generated a series of mouse strains to evaluate the relative role of HIF1α and HIF2α in regulating Treg phenotype and function. The combined loss of PHD2 and HIF2α but not HIF1α, corrected some, but not all abnormalities found in the $PHD2^{\Delta Treg}$ mouse strain. To uncover the mechanism whereby the PHD2-HIF2α axis regulates the capacity of Tregs to exert a homeostatic control over conventional T cells, a large transcriptomic analysis was undertaken. To be able to isolate genes specifically involved in the control of Treg activity in naive animals, we took advantage of the graded pro-inflammatory status of the mouse strain generated (based on colon length and spontaneous activation of Tconv cells, see **Figure 6**) to identify gene clusters whose expression correlated with Treg-mediated immune homeostasis. This analysis led us to identify important pathways providing mechanistic insights into the role of the PHD2-HIF2α axis in Treg biology. In particular, loss of PHD2 led to an altered expression of genes coding for chemokine receptors and adhesion molecules, suggesting a potential role of this oxygen sensor in chemotaxis and traffic. This conclusion is of particular interest in light of two observations described in this study. As previously discussed, $PHD2^{\Delta Treg}$ mice displayed a selective expansion of Th1-prone effectors in all lymphoid organs examined (**Figure 1**). Accordingly, ubiquitous loss of IFN-γ expression strongly attenuated the pro-inflammatory phenotype of mice with PHD2-deficient Tregs (**Figure 5-figure supplement 2**), thus suggesting a specific role for PHD2 in endowing Tregs to control Th1-like immune responses in vivo. Secondly, the IPA analysis conducted on the transcriptomic data led to the identification of STAT1 as a potential common regulator of many genes whose expression was under the control of the PHD2-HIF2α axis, including in particular CXCR3[52,60]. Based on well-described role for Treg-expressed CXCR3 in modulating Th1-like responses in vivo[61,62], and the reduced expression of this chemokine receptor described in the present study (**Figure 8e**), it is tempting to speculate that the reduced capacity of PHD2-deficient Tregs to control Th1 responses is a consequence of an altered STAT1-signaling pathway, leading to reduced CXCR3 expression. It is noteworthy that response to CXCR3 ligands has been recently shown to determine the precise positioning of effector and memory CD8 cells in peripheral lymph nodes[63]. Further studies would be required to identify the precise mechanism at work,

since the expression of many potential chemokine receptors (including CXCR4, known to exert inhibitory function over other chemokine receptors[64]) and adhesion molecules (such as Ly6a or CD44) appears under the control of the PHD2-HIF2α axis in Tregs. Whether altered positioning of Tregs within lymphoid organs represents an important factor contributing to the proinflammatory phenotype of PHD2$^{\Delta Treg}$ mice remains however to be thoroughly examined. Similarly, the potential mechanistic link between HIF2α and STAT1 activation remains to be firmly established by further investigations.

Collectively, the observations reported in this study demonstrate a non-redundant role for PHD2 in controlling survival, phenotype, migration properties and the capacity of Tregs to control Th1-like responses. These biological responses appear under the control of HIF2α, and largely independent of HIF1α-regulated metabolic pathways. Although the role of the PHD2-HIF2α axis has been previously highlighted by Yamamoto and colleagues using an alternative, shRNA-based approach[48], our observations do not fully concur with the previous study on two grounds. First, in contrast to PHD2 knock-down (PHD2-KD) cells, PHD2-genetically deficient Tregs retained full suppressive capacities in vitro. Secondly, no sign of reversal to an effector state were found in PHD2-KO regulatory T cells, whereas downregulation of PHD2 expression led to an increased expression of T-bet, GATA-3 and TNFα. Notably, PHD2-KD Tregs were able to induce skin-graft rejection in the absence of bona-fide effector cells, suggesting a possible acquisition of effector function by these cells. Although these observations are compatible with a possible gene-dosage effect of PHD2 on Treg biology, further studies are needed to identify the mechanism at work in these two experimental models.

In any events, both studies concur in identifying a possible deleterious role of HIF2α overactivation in the control of regulatory T cell function. These findings appear at odds with a recent publication by Tzu-Sheng Hsu and colleagues in which deletion of HIF2α, but not HIF1α, expression was found to negatively affect Treg function[47]. Of note, concomitant deletion of both HIF1α and HIF2α restored the suppressive activity of Tregs[47]. An elegant hypothesis, put forward by these authors, may help reconcile some of these apparently contradictory observations. Most experimental evidence concurs with a dual role of HIF1α in Treg differentiation and stability. In setting of sub-optimal Treg-inducing conditions, HIF1α may promote adequate expression of Foxp3 by differentiating Tregs. Once the Treg phenotype has been fully acquired, HIF1α protein expression is reduced following interaction with Foxp3[46], thus explaining the relative lack of influence of HIF1α on differentiated Tregs. As a consequence, HIF1α-KO Tregs retain full suppressive activity[47]. The interaction between HIF1α and Foxp3 can however also lead to Foxp3 protein degradation, and thus Treg instability. Therefore, forced stabilization of HIF1α (such as observed in triple PHD KOs[43] or pVHL-deficient Tregs[65]) leads to loss of Foxp3 expression and Treg identity and acquisition of pro-inflammatory functions. Inflammation observed in these mouse strains can be largely attributed to the

pro-inflammatory influence of ex-Tregs. As discussed for HIF1α, HIF2α also appears to regulate Treg stability, albeit in a different direction. Despite a normal phenotype at rest, mice displaying HIF2α-deficient Tregs were largely defective in suppressing inflammation in the gut and in the lungs[47]. This pro-inflammatory phenotype was largely explained by the HIF1α-dependent reprogramming of HIF2α-deficient Tregs into IL-17 secreting cells. Collectively, the available literature points to a central role for HIF1α in determining Treg stability and function in vivo. Depending on the biological pathway leading to its increased expression and/or protein stabilization, HIF1α promotes the differentiation of Tregs into IFN-γ (in triple PHD KOs or pVHL-deficient Tregs) or IL-17 (in HIF2α-deficient Tregs) secreting cells. Although the mechanism underlying the acquisition of Th1 vs Th17-like profiles in these models remains to be established, the induction of a glycolytic metabolism is probably instrumental in mediating Treg instability[66].

In the present study, loss of HIF1α expression did not revert the phenotype of PHD2-HIF2α-deficient Tregs, despite reestablishing a control-like expression of pro-glycolytic genes (**Figure 7e**). Accordingly, PHD2-deficient Tregs did not acquire the capacity to produce pro-inflammatory cytokines (**Figure 1-figure supplement 1**), nor displayed any significant loss of Foxp3 expression upon in vitro culture (**Figure 2k, l**) or in vivo transfer (**Figure 4e**). Thus, the available evidence suggests that in PHD2-sufficient cells, HIF2α allows adequate Treg function by negating the influence of HIF1α on Foxp3-expression, while overactivation of HIF2α activity secondary to the loss of PHD2 expression leads to altered Treg phenotype, most probably via a STAT1-dependent pathway.

Considering the specific role of PHD2, it is worth mentioning that both the transcriptomic data and our own unpublished observations (indicating an increased sensitivity of triple PHD2-HIF1α-HIF2α Tregs specific KO mice to chemical induced colitis) suggest that while the capacity of Tregs to control tissue homeostasis in the naive state is under the predominant control of the PHD2-HIF2α axis, other, non-HIFs PHD2-substrates[30–37]probably play an important role in Treg biology under strong inflammatory settings. Finally, the present study suggests that some caution should be exerted in the administration of PHD inhibitors presently considered for the treatment of renal anemia[67], inflammatory bowel diseases[68] as well as Parkinson's disease[69], as these compounds may display some pro-inflammatory effects via the alteration of Treg phenotype and function in vivo.

Methods

Key Resources Table				
Reagent type (species) or resource	**Designation**	**Source or reference**	**Identifiers**	**Additional information**
Genetic reagent (*M. musculus*)	C57BL/6	Envigo	RRID:MGI:5658455	Horst, The Netherlands
Genetic reagent (*M. musculus*)	*Egln1*$^{f/f}$	The Jackson Laboratory	RRID:IMSR_NM-CKO-2100497	P. Carmeliet (VIB-KULeuven)
Genetic reagent (*M. musculus*)	*Foxp3*-Cre-YFP	PMID: 18387831	RRID:IMSR_JAX:016959	A. Liston (KULeuven)
Genetic reagent (*M. musculus*)	*Hif1a*$^{f/f}$ (Hif1atm3Rsjo/J)	The Jackson Laboratory	RRID:IMSR_JAX:007561	F. Bureau (Liege University)
Genetic reagent (*M. musculus*)	*Epas*$^{f/f}$ (Epas1tm1Mcs/J)	The Jackson Laboratory	RRID:IMSR_JAX:008407	J.A. Lopez (Madrid University)
Genetic reagent (*M. musculus*)	*Ifng*$^{-/-}$	The Jackson Laboratory	RRID:IMSR_CARD:178	Bar Harbor, ME, USA
Genetic reagent (*M. musculus*)	CD45.1 (B6.SJL-Ptprca Pepcb/BoyJ)	The Jackson Laboratory	RRID:IMSR_JAX:002014	Bar Harbor, ME, USA
Genetic reagent (*M. musculus*)	*Rag2*$^{-/-}$	The Jackson Laboratory	RRID:IMSR_JAX:008449	Bar Harbor, ME, USA
Antibody	anti-mouse CD278 (Icos)-biotin (C398.4A, mouse monoclonal)	eBioscience	13-9949-82	(1:100)
Antibody	anti-mouse CD27-PeCy7 (LG.7F9, mouse monoclonal)	eBioscience	25-0271-82	(1:250)
Antibody	anti-mouse Foxp3-FITC (FJK-16s, mouse monoclonal)	eBioscience	71-5775-40	(1:100)
Antibody	anti-mouse RORγt-PE (B2D, mouse monoclonal)	eBioscience	12-6981-82	(1:100)
Antibody	anti-mouse T-bet-PE (4B10,	eBioscience	12-5825-82	(1:100)

	mouse monoclonal)			
Antibody	anti-mouse PD1-PECF594 (J43, mouse monoclonal)	BD Biosciences	562523 RRID : AB_2737634	(1:100)
Antibody	anti-mouse CXCR3-APC (CXCR3-173, mouse monoclonal)	BD Biosciences	562266 RRID : AB_11153500	(3:500)
Antibody	anti-mouse CD24-PECF594 (M1/69, mouse monoclonal)	BD Biosciences	562477 RRID : AB_11151917	(1:100)
Antibody	anti-mouse CD25-BB515 (PC61, mouse monoclonal)	BD Biosciences	564424 RRID : AB_2738803	(1:100)
Antibody	anti-mouse CD44-PECy7 (IM7, mouse monoclonal)	BD Biosciences	560569 RRID : AB_1727484	(1:100)
Antibody	anti-mouse CD4-A700 (RM4-5, mouse monoclonal)	BD Biosciences	557956 RRID : AB_396956	(3:500)
Antibody	anti-mouse CD8-A700 (53-6.7, mouse monoclonal)	BD Biosciences	557959 RRID : AB_396959	(3:500)
Antibody	anti-mouse CD4-PB (RM4-5, mouse monoclonal)	BD Biosciences	558107 RRID : AB_397030	(1:100)
Antibody	anti-mouse CD62L-A700 (MEL-14, mouse monoclonal)	BD Biosciences	560517 RRID : AB_1645210	(1:100)
Antibody	anti-mouse GATA3-PE (L50-823, mouse monoclonal)	BD Biosciences	560074 RRID : AB_1645330	(1:10)
Antibody	anti-mouse RORγt-PECF594	BD Biosciences	562684 RRID : AB_2651150	(1:200)

	(Q31-378, mouse monoclonal)			
Antibody	anti-mouse STAT1 (pY701)-A488(4a, mouse monoclonal)	BD Biosciences	612596 RRID : AB_399879	(1:10)
Antibody	anti-mouse IFNγ-PE (XMG1.2, mouse monoclonal)	BD Biosciences	554412 RRID : AB_395376	(1:100)
Antibody	anti-mouse IL-10-APC (JES5-16E3, mouse monoclonal)	BD Biosciences	554468 RRID : AB_398558	(1:100)
Antibody	anti-mouse IL-17-PerCP-Cy5.5 (N49-653, mouse monoclonal)	BD Biosciences	560799 RRID : AB_2033981	(1:100)
Antibody	anti-CD3 antibody (2c11, mouse monoclonal)	BioXcell	145-2c11	20 µg/mouse
peptide, recombinant protein	streptavidin-PECy7.	BD Biosciences	RRID :557598 AB_10049577	(1:100)
peptide, recombinant protein	IFN-γ protein	Peprotech	315-05	50 ng/mL
Chemical compound, drug	Evans blue	Sigma	314-13-6	0.5%
Chemical compound, drug	Brefeldin-A	eBioscience	00-4506-51	(1:1000)
Chemical compound,drug	Dextran Sodium Sulfate, colitis grade (36,000 - 50,000 Da)	MP Biomedical	160110	2%
Commercial assay or kit	LIVE/DEAD kit	Invitrogen	L10119	(1:1000)
Commercial assay or kit	anti-CD90.2 beads MACS	Miltenyi	130-121-278	(1:5)
Commercial assay or kit	anti-CD4 beads MACS	Miltenyi	130-117-043	(1:3)

Sequence-based reagent	*Egln1 (PHD2)_F*	This paper	PCR primers	AGGCTATGTCC GTCACGTTG
Sequence-based reagent	*Egln1 (PHD2)_R*	This paper	PCR primers	TACCTCCACTT ACCTTGGCG
Sequence-based reagent	*Egln2 (PHD1)_F*	This paper	PCR primers	TCACGTGGACG CAGTAATCC
Sequence-based reagent	*Egln2 (PHD1)_R*	This paper	PCR primers	CGCCATGCACC TTAACATCC
Sequence-based reagent	*Egln3 (PHD3)_F*	This paper	PCR primers	AGGCAATGGTG GCTTGCTAT
Sequence-based reagent	*Egln3 (PHD3)_R*	This paper	PCR primers	GACCCCTCCGT GTAACTTGG
Sequence-based reagent	*Hif1a*_F	This paper	PCR primers	CATCAGTTGCC ACTTCCCCA
Sequence-based reagent	*Hif1a_R*	This paper	PCR primers	GGCATCCAGAA GTTTTCTCACA C
Sequence-based reagent	*Epas1 (HIF2a)_F*	This paper	PCR primers	ACGGAGGTCTT CTATGAGTTGG C
Sequence-based reagent	*Epas1 (HIF2a)_R*	This paper	PCR primers	GTTATCCATTTG CTGGTCGGC
Sequence-based reagent	*Ifng_F*	This paper	PCR primers	TGCCAAGTTTG AGGTCAACA
Sequence-based reagent	*Ifng_R*	This paper	PCR primers	GAATCAGCAGC GACTCCTTT
Sequence-based reagent	*Il12a_F*	This paper	PCR primers	CCTCAGTTTGG CCAGGGTC
Sequence-based reagent	*Il12a_R*	This paper	PCR primers	CAGGTTTCGGG ACTGGCTAAG
Sequence-based reagent	*Il10_F*	This paper	PCR primers	CCTGGGTGAGA AGCTGAAGA
Sequence-based reagent	*Il10_R*	This paper	PCR primers	GCTCCACTGCC TTGCTCTTA
Sequence-based reagent	*Il17a_F*	This paper	PCR primers	ATCCCTCAAAG CTCAGCGTGTC
Sequence-based reagent	*Il17a_R*	This paper	PCR primers	GGGTCTTCATT GCGGTGGAGA G
Sequence-based reagent	*Il1b_F*	This paper	PCR primers	CAAGCTTCCTT GTGCAAGTG
Sequence-based reagent	*Il1b_R*	This paper	PCR primers	AGGTGGCATTT CACAGTTGA
Sequence-based reagent	*Il4_F*	This paper	PCR primers	ATGCACGGAGA TGGATGTG
Sequence-based reagent	*Il4_R*	This paper	PCR primers	AATATGCGAAG CACCTTGGA
Sequence-based reagent	*Il6_F*	This paper	PCR primers	GTTCTCTGGGA AATCGTGGA

Sequence-based reagent	*Il6_R*	This paper	PCR primers	GCAAGTGCATC ATCGTTGTT
Sequence-based reagent	*Rpl32_F*	This paper	PCR primers	ACATCGGTTAT GGGAGCAAC
Sequence-based reagent	*Rpl32_R*	This paper	PCR primers	TCCAGCTCCTT GACATTGT
Sequence-based reagent	*Tnfa_F*	This paper	PCR primers	GCCTCCCTCTC ATCAGTTCTA
Sequence-based reagent	*Tnfa_R*	This paper	PCR primers	GCTACGACGTG GGCTACAG
Sequence-based reagent	*Il12b*_F	This paper	PCR primers	ATGTGTCCTCA GAAGCTAACC
Sequence-based reagent	*Il12b*_R	This paper	PCR primers	CTAGGATCGGA CCCTGCAGGGA AC
Software, algorithm	Prism 6	GraphPad	RRID:SCR_002 798	Version 6.0

Mice. C57BL/6 mice were purchased from Envigo (Horst, The Netherlands). *Egln1*$^{f/f}$ mice were provided by P. Carmeliet (VIB-KULeuven, Leuven, Belgium); *Foxp3*-Cre-YFP mice, developed by A. Rudensky [70] were kindly provided by A. Liston (KULeuven, Leuven, Belgium); Hif1atm3Rsjo/J (*Hif1a*$^{f/f}$) mice were kindly provided by F. Bureau (Liege University, Liege, Belgium); Epas1tm1Mcs/J (*Epas*$^{f/f}$) mice were provided by J.A. Lopez (Madrid University, Madrid, Spain); *Ifng*$^{-/-}$, CD45.1 (B6.SJL-Ptprc^{a} Pepc^{b}/Boy^{J}) and *Rag2*$^{-/-}$ mice were obtained from The Jackson Laboratory (Bar Harbor, ME, USA). All mice were backcrossed for more than 10 generations into a C57BL/6 background and housed in individually ventilated cages. *Foxp3*-Cre-YFP mice were crossed with *Egln1*$^{f/f}$, *Hif1a*$^{f/f}$, *Epas*$^{f/f}$ to produce mice with Treg-specific deletion of PHD2, HIF1α, HIF2α, PHD2-HIF1α, PHD2-HIF2α or PHD2-HIF1α-HIF2α. Heterozygous *Foxp3*$^{cre/+}$ *Egnl1*$^{fl/fl}$ mice were generated by crossing the *Foxp3*-Cre-YFP mice with *Egln1*$^{f/f}$ mice. All mice were used between 8 and 14 weeks of age. PHD2-sufficient mice (expressing *Foxp3*-Cre-YFP, or floxed forms of PHD2, HIF1α and HIF2α-encoding alleles and generated as littermates in our colony) were used as appropriate controls in the early stages of this work. These mice displayed a phenotype indistinguishable from WT mice and were therefore considered as a single experimental group throughout this study in order to reach statistical significance in all experiments. The experiments were carried out in compliance with the relevant laws and institutional guidelines and were approved by the Université Libre de Bruxelles Institutional Animal Care and Use Committee (protocol number CEBEA-4).

Antibodies, intracellular staining and flow cytometry. The following monoclonal antibodies were purchased from eBioscience: CD278 (ICOS)-biotin, CD27-PeCy7, Foxp3-FITC, RORγt-PE, T-bet-PE; or from BD Biosciences: PD1-PECF594, CXCR3-APC, CD24-PECF594, CD25-BB515, CD44-PECy7, CD4-A700, CD8-A700, CD4-PB,

CD62L-A700, GATA3-PE, RORγt-PECF594, STAT1 (pY701)-A488, IFNγ-PE, IL-10-APC, IL-17-PerCP-Cy5.5, streptavidin-PECy7. Live/dead fixable near-IR stain (ThermoFisher) was used to exclude dead cells. For transcription factor staining, cells were stained for surface markers, followed by fixation and permeabilization before nuclear factor staining according to the manufacturer's protocol (Foxp3 staining buffer set from eBioscience). For cytokine staining, cells were stimulated in media containing phorbol 12-myristate 13-acetate (50ng/mL, Sigma-Aldrich), ionomycin (250ng/mL, Sigma-Aldrich) and brefeldin-A (1/100, eBioscience) for 3h. After stimulation, cells were stained for surface markers, followed by fixation and permeabilization before intracellular staining according to the manufacturer's protocol (cytokine staining buffer set from BD Biosciences). For phosphorylation staining, cells were stimulated with IFN-γ (50 ng/mL, Peprotech) for 30 min, fixed with formaldehyde and permeabilized with methanol before staining. Flow cytometric analysis was performed on a Canto II (BD Biosciences) and analyzed using FlowJo software (Tree Star).

T cell cultures. After removal of Peyer's patches and mesenteric fat, intestinal tissues were washed in HBSS 3% FCS and PBS, cut in small sections and incubated in HBSS 3% FCS containing 2,5mM EDTA and 72,5 µg/mL DTT for 30 min at 37°C with agitation to remove epithelial cells, and then minced and dissociated in RPMI containing liberase (20 µg/ml, Roche) and DNase (400 µg/ml, Roche) at 37 °C for 30 min. Leukocytes were collected after a 30% Percoll gradient (GE Healthcare). Lymph nodes and spleens were mechanically disrupted in culture medium. $CD4^+$ T cells were positively selected from organ cell suspensions by magnetic-activated cell sorting using CD4 beads (MACS, Miltenyi) according to the manufacturer's protocol, and purified as $CD4^+$ $CD44^{lo}CD62L^{hi}CD25^-$ or $CD4^+$ $CD44^{lo}$ $CD62L^{hi}$ YFP^- by fluorescence activated cell sorting. T cells were cultured at 37°C in RPMI supplemented with 5% heat-inactivated FBS (Sigma-Aldrich), 1% non-essential amino acids (Invitrogen), 1 mM sodium pyruvate (Invitrogen), 2 mM L-glutamin (Invitrogen), 500 U/mL penicillin/500 µg/ml streptomycin (Invitrogen), and 50 µM β-mercaptoethanol (Sigma-Aldrich). To generate iTreg cells, cells were cultured in 24 well plates coated with 5µg/mL anti-CD3 (BioXcell, clone 145-2C11) at 37°C for 72h. The culture was supplemented with anti-CD28 (1 µg/mL, BioXcell, clone 37.51), TGF-β (3 ng/ml, eBioscience) and IL-2 (10 ng/mL, Peprotech) for optimal iTreg cell polarization.

Treg cell suppression assays. *In vitro assay*: $CD4^+$ $CD44^{lo}CD62L^{hi}$ $CD25^-$ naive T cells were isolated from the spleen of $CD45.1^+$ mice by cell sorting after positive enrichment for $CD4^+$ cells using MACS LS columns (Miltenyi) and labelled with carboxyfluorescein diacetate succinimidyl ester (CFSE, ThermoFisher). $CD4^+YFP^+$ Treg cells were isolated from the spleen of $Foxp3^{cre}$ or $PHD2^{\Delta Treg}$ mice by cell sorting. Splenocytes from wild-type B6 mice were depleted in T cells (anti-CD90.2 beads, MACS, Miltenyi) using MACS LS columns (Miltenyi) and used as feeder cells. 4×10^4 CFSE-labelled naive T cells were cultured for 72 h with feeder cells (1×10^5) and

soluble anti-CD3 (0,5 µg/mL) in the presence or absence of various numbers of Treg cells as indicated.

In vivo assay: *Rag2*$^{-/-}$ mice were injected i.v with a mixture of naive, CFSE labeled, CD4^{+} T cells (CD45.1^{+} CD4^{+} CD44^{lo} CD62L^{hi} CD25^{-}) (1 x 10^{6}) and splenic Treg from Foxp3^{cre} or PHD2$^{\Delta Treg}$ mice (3.3 x 10^{5}). Six days after the injection, *Rag2*$^{-/-}$ mice were sacrificed and CD4^{+} T cells proliferation and activation analyzed by flow cytometry.

DSS-induced colitis. Foxp3^{cre} or PHD2$^{\Delta Treg}$ mice were provided with 2% DSS (MP Biomedical, 160110) in tap water for five days. On day 5, the DSS-containing water was replaced with normal drinking water and mice were followed during 14 days for body weight, survival, and colitis severity. Colitis severity score was assessed by examining weight loss, feces consistency and hematochezia (Hemoccult SENSA, Mckesson Medical-Surgical, 625078) as described in ref [71]. Colon samples were washed with PBS and rolled from the distal to proximal end, transected with a needle and secured by bending the end of the needle and fixed in fresh 4% paraformaldehyde (Sigma-Aldrich) overnight and further subjected to routine histological procedures for embedment in paraffin and hematoxylin and eosin (H&E) staining. Tissues were analyzed and scored in a blinded fashion by an independent histopathologist and representative images were subsequently chosen to illustrate key histological findings.

Toxoplasma infection. ME-49 type II *Toxoplasma gondii* was kindly provided by Dr De Craeye (Scientific Institute of Public Health, Belgium) and was used for the production of tissue cysts in C57BL/6 mice previously (1-3 month) inoculated with three cysts by gavage. Animals were killed, and the brains were removed. Tissue cysts were counted and mice were infected by intragastric gavage with 10 cysts. Mice were sacrificed at day 8 after infection.

Anti-CD3 mAb-induced enteritis. Mice were injected i.p. with a CD3-specific antibody (clone 145-2C11, BioXcell 20 µg/mouse) on days 0 and 2 and weighted daily. Mice were sacrificed on day 3 and cytokine production evaluated by qPCR as indicated in the figure legend.

Hematological analysis. Mice blood was obtained from the submandibular vein and collected into heparin prefilled tubes. Blood samples were analyzed using a Sysmex KX-21 N Automated Hematology Analyzer.

Evans blue assay. Blood vessel permeability was assesed as previously described[72]. Briefly, 200 µL of a 0.5% sterile solution of Evans blue (Sigma) in PBS was i.v injected in mice. After 30 min, organs were colleted, weighted and were put in formamide. After 24 hours in a 55°C water bath, absorbance was mesuread at 600 nm.

RT-qPCR. RNA was extracted using the TRIzol method (Invitrogen) and reverse transcribed with Superscript II reverse transcriptase (Invitrogen) according to the manufacturer's instructions. Quantitative real-time RT-PCR was performed using the SYBR Green Master mix kit (ThermoFisher). Primer sequences were as follows:

Rpl32 (F) ACATCGGTTATGGGAGCAAC; *Rpl32* (R) TCCAGCTCCTTGACATTGT; *Il1b* (F) CAAGCTTCCTTGTGCAAGTG; *Il1b* (R) AGGTGGCATTTCACAGTTGA; *Il10* (F) CCTGGGTGAGAAGCTGAAGA; *Il10* (R) GCTCCACTGCCTTGCTCTTA; *Ifng* (F) TGCCAAGTTTGAGGTCAACA; *Ifng* (R) GAATCAGCAGCGACTCCTTT; *Il6* (F) GTTCTCTGGGAAATCGTGGA; *Il6* (R) GCAAGTGCATCATCGTTGTT; *Il17a* (F) ATCCCTCAAAGCTCAGCGTGTC; *Il17a* (R) GGGTCTTCATTGCGGTGGAGAG; *Il12a* (F) CCTCAGTTTGGCCAGGGTC; *Il12a* (R) CAGGTTTCGGGACTGGCTAAG; *Il12b* (F) ATGTGTCCTCAGAAGCTAACC; *Il12b* (R) CTAGGATCGGACCCTGCAGGGAAC; *Tnfa* (F) GCCTCCCTCTCATCAGTTCTA; *Tnfa* (R) GCTACGACGTGGGCTACAG; *Egln1* (F) AGGCTATGTCCGTCACGTTG; *Egln1* (R) TACCTCCACTTACCTTGGCG; *Hif1a* (F) CATCAGTTGCCACTTCCCCA; *Hif1a* (R) GGCATCCAGAAGTTTTCTCACAC; *Epas1* (F) ACGGAGGTCTTCTATGAGTTGGC; *Epas1* (R) GTTATCCATTTGCTGGTCGGC.

RNA Sequencing and analysis. All RNA-Seq analyses were performed using ≥ 2 biological replicates. Total RNA was prepared from purified splenic Treg cells using the TRIzol method (Invitrogen). 200 ng of total RNA was subsequently used to prepare RNA-Seq library by using TruSeq RNA sample prep kit (Illumina) according to manufacturer's instructions. Paired-end RNA sequencing was performed on a Novaseq 6000 (Illumina) (BRIGHTcore joint facility, ULB-VUB, Brussels, Belgium). Sequenced reads were aligned to the mouse genome (NCBI37/mm9) and uniquely mapped reads were used to calculate gene expression. Data analysis was performed using R program (Deseq2 package). Differentially expressed genes are considered significant when the FDR (false discovery rate or adjusted p-value) < 0.05 and the $\log_2$FC (fold change) > 0.5. Upstream regulators analysis was performed following Ingenuity pathway analysis (IPA). IPA predicts functional regulatory networks from gene expression data and provides a significance score (p-value) for each network according to the fit of the network to the set of genes in the database.

Statistical analysis. All statistical analyses were conducted using GraphPad Prism (GraphPad Software). Statistical difference between two groups was determined by an unpaired, two-tailed student's t tests. A one-way or two-way ANOVA was used for multigroup comparisons together with Tukey's multiple comparisons post hoc tests. Survival significance in DSS-induced colitis was determined by a Log-rank Mantel-Cox test. Data is judged to be statistically significant when p value < 0.05. In figures, asterisks denote statistical significance (*, $p < 0.05$; **, $p < 0.01$; ***, $p < 0.001$; ****, $p < 0.0001$).

References

1. Lu, L., Barbi, J. & Pan, F. The regulation of immune tolerance by FOXP3. *Nat. Rev. Immunol.* **17**, 703–717 (2017).
2. Xing, Y. & Hogquist, K. A. T-Cell Tolerance: Central and Peripheral. *Cold Spring Harb Perspect Biol* **4**, 1–15 (2012).
3. Dominguez-Villar, M. & Hafler, D. A. Regulatory T cells in autoimmune disease. *Nat. Immunol.* **19**, 665–673 (2018).
4. Samstein, R. M., Josefowicz, S. Z., Arvey, A., Treuting, P. M. & Rudensky, A. Y. Extrathymic generation of regulatory T cells in placental mammals mitigates maternal-fetal conflict. *Cell* **150**, 29–38 (2012).
5. Togashi, Y., Shitara, K. & Nishikawa, H. Regulatory T cells in cancer immunosuppression - implications for anticancer therapy. *Nat. Rev. Clin. Oncol.* (2019).
6. Aandahl, E. M., Michaëlsson, J., Moretto, W. J., Hecht, F. M. & Nixon, D. F. Human CD4+ CD25+ Regulatory T Cells Control T-Cell Responses to Human Immunodeficiency Virus and Cytomegalovirus Antigens. *J. Virol.* **78**, 2454–2459 (2004).
7. Van Der Burg, S. H. *et al.* Association of cervical cancer with the presence of CD4+ regulatory T cells specific for human papillomavirus antigens. *PNAS* **104**, 12087–12092 (2007).
8. Caridade, M., Graca, L. & Ribeiro, R. M. Mechanisms underlying CD4+ Treg immune regulation in the adult: From experiments to models. *Front. Immunol.* **4**, 1–9 (2013).
9. Clement, R. L. *et al.* Follicular regulatory T cells control humoral and allergic immunity by restraining early B cell responses. *Nat. Immunol.* **20**, 1360–1371 (2019).
10. Vignali, D. A. A., Collison, L. W. & Workman, C. J. How regulatory T cells work. *Nat. Rev. Immunol.* **8**, 523–532 (2008).
11. Wardell, C. M., MacDonald, K. N., Levings, M. K. & Cook, L. Cross talk between human regulatory T cells and antigen-presenting cells: Lessons for clinical applications. *Eur. J. Immunol.* **51**, 27–38 (2021).
12. Shevyrev, D. & Tereshchenko, V. Treg Heterogeneity, Function, and Homeostasis. *Front. Immunol.* **10**, 1–13 (2020).
13. Panduro, M., Benoist, C. & Mathis, D. Tissue Tregs. *Annu. Rev. Immunol.* **34**, 609–633 (2016).
14. Ast, T. & Mootha, V. K. Oxygen and mammalian cell culture: are we repeating the experiment of Dr. Ox? *Nat. Metab.* **1**, 858–860 (2019).
15. McKeown, S. R. Defining normoxia, physoxia and hypoxia in tumours - Implications for treatment response. *Br. J. Radiol.* **87**, 1–12 (2014).
16. Bartels, K., Grenz, A. & Eltzschig, H. K. Hypoxia and inflammation are two sides of the same coin. *PNAS* **110**, 18351–18352 (2013).
17. Nanduri, J. *et al.* HIF-1α activation by intermittent hypoxia requires NADPH oxidase stimulation by xanthine oxidase. *PLoS One* **10**, 1–12 (2015).
18. Mempel, T. R. & Marangoni, F. Guidance factors orchestrating regulatory T cell positioning in tissues during development, homeostasis, and response. *Immunol.*

Rev. **289**, 129–141 (2019).
19. Hirota, K. Basic biology of hypoxic responses mediated by the transcription factor HIFs and its implication for medicine. *Biomedicines* **8**, (2020).
20. Baik, A. H. & Jain, I. H. Turning the Oxygen Dial: Balancing the Highs and Lows. *Trends Cell Biol.* **30**, 516–536 (2020).
21. Wang, G. L. & Semenza, G. L. Purification and characterization of hypoxia-inducible factor. *Journal of Biological Chemistry* **270**, 1230–1237 (1995).
22. James D Webb, M. L. C. & Pugh, C. W. Hypoxia, hypoxia-inducible factors (HIF), HIF hydroxylases and oxygen sensing. *Cell. Mol. Life Sci.* **66**, 3539–3554 (2009).
23. Semenza, G. L. HIF-1, O2, and the 3 PHDs: How animal cells signal hypoxia to the nucleus. *Cell* **107**, 1–3 (2001).
24. Maxwell, P. H. *et al.* The tumoursuppressor proteinVHLtargets hypoxia-inducible factors for oxygen-dependent proteolysis. *Nature* **44**, 271–275 (1999).
25. Downes, N. L., Laham-Karam, N., Kaikkonen, M. U. & Ylä-Herttuala, S. Differential but Complementary HIF1α and HIF2α Transcriptional Regulation. *Mol. Ther.* **26**, 1735–1745 (2018).
26. Watts, E. R. & Walmsley, S. R. Inflammation and Hypoxia: HIF and PHD Isoform Selectivity. *Trends Mol. Med.* **25**, 33–46 (2019).
27. Talks, K. L. *et al.* The expression and distribution of the hypoxia-inducible factors HIF-1α and HIF-2α in normal human tissues, cancers, and tumor-associated macrophages. *Am. J. Pathol.* **157**, 411–421 (2000).
28. Hu, C.-J., Sataur, A., Wang, L., Chen, H. & Simon, M. C. The N-Terminal Transactivation Domain Confers Target Gene Specificity of Hypoxia-inducible Factors HIF-1α and HIF-2α. *Mol. Biol. Cell* **18**, 986–994 (2007).
29. Bono, H. & Hirota, K. Meta-analysis of hypoxic transcriptomes from public databases. *Biomedicines* **8**, (2020).
30. Meneses, A. M. and & Wielockx, B. PHD2 : from hypoxia regulation to disease progression. *Dovepress* 53–67 (2016).
31. Mikhaylova, O. *et al.* The von Hippel-Lindau Tumor Suppressor Protein and Egl-9-Type Proline Hydroxylases Regulate the Large Subunit of RNA Polymerase II in Response to Oxidative Stress. *Mol. Cell. Biol.* **28**, 2701–2717 (2008).
32. Denise A. Chan *et al.* Tumor Vasculature is Regulated by PHD2-mediated Angiogenesis and Bone Marrow-Derived Cell Recruitment. *Cancer Cell.* **15**, 527–538 (2009).
33. Romero-Ruiz, A. *et al.* Prolyl hydroxylase-dependent modulation of eukaryotic elongation factor 2 activity and protein translation under acute hypoxia. *J. Biol. Chem.* **287**, 9651–9658 (2012).
34. Huo, Z. *et al.* Prolyl hydroxylase domain protein 2 regulates the intracellular cyclic AMP level in cardiomyocytes through its interaction with phosphodiesterase 4D. *Biochem. Biophys. Res. Commun.* **427**, 73–79 (2012).
35. Xie, L. *et al.* PHD2/3-dependent hydroxylation tunes cardiac response to β-adrenergic stress via phospholamban. *J. Clin. Invest.* **125**, 2759–2771 (2015).
36. Lee, D. C. *et al.* A lactate-induced response to hypoxia. *Cell* **161**, 595–609 (2015).
37. Guo, J. *et al.* pVHL suppresses kinase activity of Akt in a proline-hydroxylation–dependent manner. *Science.* **353**, 929–932 (2016).
38. Corrado, C. & Fontana, S. Hypoxia and HIF signaling: One axis with divergent effects. *Int. J. Mol. Sci.* **21**, 1–17 (2020).

39. McGettrick, A. F. & O'Neill, L. A. J. The Role of HIF in Immunity and Inflammation. *Cell Metab.* **32**, 524–536 (2020).
40. Shi, L. Z. *et al.* HIF1alpha-dependent glycolytic pathway orchestrates a metabolic checkpoint for the differentiation of TH17 and Treg cells. *J. Exp. Med.* **208**, 1367–76 (2011).
41. Dang, E. V. *et al.* Control of TH17/Treg balance by hypoxia-inducible factor 1. *Cell* **146**, 772–784 (2011).
42. Shehade, H., Acolty, V., Moser, M. & Oldenhove, G. Cutting Edge: Hypoxia-Inducible Factor 1 Negatively Regulates Th1 Function. *J. Immunol.* **195**, 1372–6 (2015).
43. Clever, D. *et al.* Oxygen Sensing by T Cells Establishes an Immunologically Tolerant Metastatic Niche. *Cell* **166**, 1117-1131.e14 (2016).
44. Lukashev, D., Caldwell, C., Ohta, A., Chen, P. & Sitkovsky, M. Differential Regulation of Two Alternatively Spliced Isoforms of Hypoxia-inducible Factor-1α in Activated T Lymphocytes. *J. Biol. Chem.* **276**, 48754–48763 (2001).
45. Ben-shoshan, J., Maysel-auslender, S., Mor, A., Keren, G. & George, J. Hypoxia controls CD4+ CD25+ regulatory T-cell homeostasis via hypoxia-inducible factor-1 a. *Eur. J. Immunol.* 2412–2418 (2008).
46. Clambey, E. T. *et al.* Hypoxia-inducible factor-1 alpha – dependent induction of FoxP3 drives regulatory T-cell abundance and function during inflammatory hypoxia of the mucosa. *PNAS* **109**, (2012).
47. Hsu, T. S. *et al.* HIF-2α is indispensable for regulatory T cell function. *Nat. Commun.* **11**, 1–16 (2020).
48. Yamamoto, A. *et al.* Systemic silencing of Phd2 causes reversible immune regulatory dysfunction. *J. Clin. Invest.* **129**, 3640–3656 (2019).
49. Owen, D. L. *et al.* Thymic regulatory T cells arise via two distinct developmental programs. *Nat. Immunol.* **20**, 195–205 (2019).
50. Wohlfert, E. A., Warunek, J., Jin, R. M. & Marzullo, B. Tbet - expressing Tregs protect against lethal immunopathology during T . gondii infection. *J Immunol* **204**, 2020 (2020).
51. Esplugues, E. *et al.* Control of TH17 cells occurs in the Small Intestine. *Nature* **475**, 514–518 (2012).
52. Hall, A. O. H. *et al.* The Cytokines Interleukin 27 and Interferon-γ Promote Distinct Treg Cell Populations Required to Limit Infection-Induced Pathology. *Immunity* **37**, 511–523 (2012).
53. Fontenot, J. D., Gavin, M. A. & Rudensky, A. Y. Foxp3 programs the development and function of CD4+CD25+ regulatory T cells. *J. Immunol.* **4**, 986–992 (2003).
54. Redpath, S. A. *et al.* ICOS controls Foxp3+ regulatory T-cell expansion, maintenance and IL-10 production during helminth infection. *Eur. J. Immunol.* **43**, 705–715 (2013).
55. Lowther, D. E. *et al.* PD-1 marks dysfunctional regulatory T cells in malignant gliomas. *JCI* **1**, 1–15 (2016).
56. Tan, C. L. *et al.* PD-1 restraint of regulatory T cell suppressive activity is critical for immune tolerance. *J. Exp. Med.* **218**, (2021).
57. Bates, D. O. Vascular endothelial growth factors and vascular permeability. *Cardiovasc. Res.* **87**, 262–271 (2010).
58. Greenwald, A. C. *et al.* VEGF expands erythropoiesis via hypoxia-independent

induction of erythropoietin in noncanonical perivascular stromal cells. *J. Exp. Med.* **216**, 215–230 (2019).
59. Franckaert, D. *et al.* Promiscuous Foxp3-cre activity reveals a differential requirement for CD28 in Foxp3 + and Foxp3-T cells. *Immunol. Cell Biol.* **93**, 417–423 (2015).
60. Koch, M. A. *et al.* The transcription factor T-bet controls regulatory T cell homeostasis and function during type 1 inflammation. *Nat. Immunol.* **10**, 595–602 (2009).
61. Levine, A. G. *et al.* Stability and function of regulatory T cells expressing the transcription factor T-bet. *Nature* **546**, 421–425 (2017).
62. Littringer, K. *et al.* Common features of regulatory T cell specialization during Th1 responses. *Front. Immunol.* **9**, 1–15 (2018).
63. Duckworth, B. C. *et al.* Effector and stem-like memory cell fates are imprinted in distinct lymph node niches directed by CXCR3 ligands. *Nat. Immunol.* (2021).
64. Biasci, D. *et al.* CXCR4 inhibition in human pancreatic and colorectal cancers induces an integrated immune response. *PNAS* **117**, 28960–28970 (2020).
65. Lee, J. H., Elly, C., Park, Y. & Liu, Y. C. E3-Ubiquitin Ligase VHL Regulates Hypoxia-Inducible Factor-1a to Maintain Regulatory T Cell Stability and Suppressive Capacity. *Immunity* **42**, 1062–1074 (2015).
66. Shi, H. & Chi, H. Metabolic Control of Treg Cell Stability, Plasticity, and Tissue-Specific Heterogeneity. *Front. Immunol.* **10**, 1–17 (2019).
67. Gupta, N. & Wish, J. B. Hypoxia-Inducible Factor Prolyl Hydroxylase Inhibitors: Potential New Treatment for Anemia in Patients With CKD. *Am. J. Kidney Dis.* **69**, 815–826 (2017).
68. Marks, E. *et al.* Oral Delivery of Prolyl Hydroxylase Inhibitor : AKB-4924 Promotes Localized Mucosal Healing in a Mouse Model of Colitis. *Inflamm Bowel Dis* **21**, 267–275 (2015).
69. Li, X. *et al.* Therapeutic Potential of a Prolyl Hydroxylase Inhibitor FG-4592 for Parkinson ' s Diseases in Vitro and in Vivo : Regulation of Redox Biology and Mitochondrial Function. *Frontiers (Boulder).* **10**, 1–16 (2018).
70. Rubtsov, Y. P. *et al.* Regulatory T Cell-Derived Interleukin-10 Limits Inflammation at Environmental Interfaces. *Immunity* **28**, 546–558 (2008).
71. Kim, J. J., Shajib, S., Manocha, M. M. & Khan, W. I. Investigating Intestinal Inflammation in DSS-induced Model of IBD. *Jove* **1**, 1–6 (2012).
72. Radu, M. & Chernoff, J. An in vivo assay to test blood vessel permeability. *J. Vis. Exp.* 2–5 (2013).

Acknowledgments

We thank Valérie Acolty, Caroline Abdelaziz and Véronique Dissy for animal care and for technical support. The development of mouse models of toxoplasmosis would not have been possible without the kind assistance of Guillaume Oldenhove. This work was supported by the European Regional Development Fund (ERDF) and the Walloon Region (Wallonia-Biomed portfolio, 411132- 957270), a grant from the Fonds Jean Brachet and research credit from the National Fund for Scientific Research, FNRS, Belgium. FA is a Research Associate at the FNRS. YA is recipient of a research fellowship from the FNRS/Télévie. HH has been supported by a Belgian FRIA fellowship.

Additional information

The authors declare that the research was conducted in the absence of any commercial or financial relationships that could be construed as a potential conflict of interest.

Figure legends

Figure 1. PHD2$^{\Delta Treg}$ mice display a spontaneous Th1-like inflammatory syndrome. **a** Body weight of naive mice was determined weekly. **b** At 12 weeks of age, male and female mice were examined for rectal prolapse **c** splenomegaly and colon length summarized in **d**. **e** Representative gross autopsy of an hemorrhagic abdomen, (**f-i**) Lymphoid cells from spleen, mesenteric (mLN), peripheral (pLN) lymph nodes or the small intestine lamina propria were collected from Foxp3^{cre} and PHD2$^{\Delta Treg}$ mice. **f** Frequency of conventional, Foxp3- CD4 and CD8-expressing cells among TCRβ-expressing T lymphocytes. **g** Representative merged (n = 15) t-distributed stochastic neighbor embedding (t-SNE) plot after dimensionality reduction and unsupervised clustering of flow cytometry data from CD4-expressing spleen cells. Relative distributions of CD4^{+} lymphocyte subsets are shown as doughnut charts. **h** Frequency of effector-like (CD44^{hi} CD62L^{lo}) conventional T lymphocytes in the indicated lymphoid organs. **i** Frequency of IFN-γ (top panel) and IL-17A (bottom panel) producing CD4^{+} T cells after in vitro stimulation. **j** Expression of inflammatory cytokines determined by qPCR on extracts from unfractionated mLNs. Data are representative of at least three independent experiments with n = 9 (**a, j**), n = 25 (**d**), n = 15 (**f-i**) per group. Values are presented as the mean ± standard deviation (SD) and were compared by two-tailed unpaired student's t-test. Only significant differences are indicated as follows: *: $p<0.05$, **: $p<0.01$, ***: $p<0.001$, ****: $p<0.0001$. Abbreviations: Naive Tconv (Foxp3^{-} CD44^{-} CD62L^{+}), Memory Tconv (Foxp3^{-} CD44^{+} CD62L^{+}), Effector Tconv (Foxp3^{-} CD44^{+} CD62L^{-}), Memory Treg (Foxp3^{+} CD44^{+}CD62L^{+}), Effector Treg (Foxp3^{+} CD44^{+}CD62L^{-}).

Figure 2. Increased number, but altered phenotype of PHD2-deficient Treg cells. Lymphoid cells from the thymus, spleen, mesenteric (mLN) and peripheral (pLN) lymph nodes were collected at 12 weeks of age from Foxp3^{cre} and PHD2$^{\Delta Treg}$ male and female mice and the relative frequency and phenotype of Foxp3-expressing cells were established by flow cytometry or qPCR. **a** Frequency of Foxp3-expressing cells among CD4-positive T lymphocytes; **b** Representative flow cytometry expression profiles of Foxp3 and CD25 expression among thymic CD4^{+} T cells; **c** frequency of mature-like (CD25^{+} Foxp3^{+}) and Treg precursors subsets identified respectively as CD25^{-} Foxp3^{lo} and CD25^{+} Foxp3^{-} cells among thymic CD4^{+} T cells; **d** frequency of immature-like, CD24^{+} Foxp3^{+} T cells in the thymus of adult mice; **e** frequency of effector (CD62L^{low} CD44^{high}), memory (CD62L^{high} CD44^{high}) and naive (CD62L^{high} CD44^{low}) splenic Foxp3-expressing cells; **f** frequency of splenic Tregs expressing the master transcription factors T-bet, GATA3 and RORγt; **g** Ratio of the Foxp3 MFI of PHD2-KO splenic Tregs to Foxp3^{cre} splenic Tregs. **h** Expression of CD25, CD44, ICOS, PD-1 and CTLA-4 in splenic Treg of Foxp3^{cre} and PHD2$^{\Delta Treg}$ mice. Top panel, representative traces of MFI. Bottom panel, ratios of the MFIs of PHD2-KO Treg to Foxp3^{cre} Treg cells are expressed as the mean ± SD. **i** *Il10* gene expression relative to RPL32 by ex-vivo purified Tregs was determined by qPCR. (**j-l**) CD4^{+} Foxp3^{-} splenic naive T cells were stimulated in

vitro with anti-CD3/CD28 (5/1μg ml^{-1}) in the presence of TGF-β (3 μg ml^{-1}) and IL-2 (10 μg ml^{-1}) for 72h to induce Treg polarization.
j Representative flow cytometry expression profiles of Foxp3 expression at the end of the culture period. The first panel represents a typical profile of cells activated in the absence of polarizing cytokines; **k** number of $Foxp3^+$ cells generated in the culture conditions; **l** Expression (MFI) of Foxp3 by in vitro induced Treg cells. Data are representative of at least two independent experiments with n = 15 (**a, e-g**), n = 9 (**h, i**) or n = 6 (**c, d, k, l**) per group. Values are presented as the mean ± SD and were compared by two-tailed unpaired student's t-test. Only significant differences are indicated as follows: *: p<0.05, **: p<0.01, ***: p<0.001.

Figure 3. Cell autonomous role of PHD2 in determining Treg cells phenotype.
Spleen, thymus, mesenteric (mLN) and peripheral (pLN) lymph nodes were collected at 8 weeks of age from *Foxp3*$^{cre/+}$ *Egln1*$^{f/f}$ heterozygous female mice and the relative frequency and phenotype of Foxp3-expressing cells were established by flow cytometry. **a** Proportion of WT (YFP- cells) or PHD2-KO (YFP+ cells) Treg cells among Foxp3-expressing cells. **b** representative histograms of Foxp3, CD25, CD44 and CTLA-4 expression in splenic WT Tregs (black lines) compared to splenic PHD2-KO Tregs (red lines). **c** Foxp3 MFI, **d** CD25 MFI, **e** CD44 MFI and **f** CTLA-4 MFI of WT and PHD2-KO Tregs in lymphoid organs. Data are representative of two independent experiments with n = 9 per group. Values are presented as the mean ± standard deviation (SD) and were compared by two-tailed unpaired student's t-test. Only significant differences are indicated as follows: *: p<0.05, **: p<0.01, ***: p<0.001, ****: p<0.0001.

Figure 4. Reduced in vivo but not in vitro suppressive capacity of PHD2-deficient Treg.
a Treg function was assayed following adoptive co-transfer of CD45.2 Foxp3-expressing cells with naive, CFSE labeled congenic CD45.1 $CD4^+$ lymphocytes (Treg : Tconv ratio 1:3) into syngeneic lymphopenic male mice (*Rag2*$^{-/-}$). Recipient mice were euthanized at day 6 post-transfer, and their spleen and mLN cells analyzed by flow cytometry. **b** Representative flow cytometry expression profiles of CFSE labeled cells (CD45.1 gate in the spleen) with or without co-transferred $Foxp3^+$ cells from $Foxp3^{cre}$ or $PHD2^{\Delta Treg}$ male mice; **c** percentage of suppression established from CFSE staining profiles; **d** frequency of activated ($CD4^+$ $CD45.1^+$ $CD44^{hi}$ $CD62L^{lo}$) cells in the indicated lymphoid organs; **e** frequency of Treg cells in the indicated organs 6 days post-transfer. (**f, g**) CFSE-labeled, naive conventional $CD4^+$ T cells from CD54.1 mice were co-cultured with ex-vivo purified Treg cells from $Foxp3^{cre}$ or $PHD2^{\Delta Treg}$ mice at the indicated ratios in the presence of anti-CD3 antibodies (0.5 μg ml^{-1}) and splenic feeder cells; **f** representative flow cytometry profiles of CSFE staining; **g** Percent of suppression of proliferation as compared to cultures in which Treg cells were omitted. Data are representative of three independent experiments with n = 15 (**b-e**) or n = 4 (**f, g**) per group. Values are presented as the mean ± SD and were compared by two-way ANOVA with Tukey's multiple comparisons test (**c-e**) or by two-tailed unpaired student's t-test (**g**). Only significant differences are indicated as follows: *: p<0.05, **: p<0.01, ***: p<0.001.

Figure 5. Increased sensitivity of PHD2$^{\Delta Treg}$ mice to DSS-induced colitis and toxoplasmosis.
Foxp3^{cre} and PHD2$^{\Delta Treg}$ male mice were provided with 2% DSS in tap water for five days. On day 5, the 2% DSS water was replaced with normal drinking water and mice were followed during 14 days for **a** body weight, **b** survival, **c** colitis severity and **d** colon length. **e** Colons were isolated from untreated mice or 6 days after colitis induction and were fixed and stained with hematoxylin and eosin (H&E); arrows indicate inflammatory cell infiltrates. **f** Foxp3^{cre} and PHD2$^{\Delta Treg}$ male mice were infected by intragastric gavage with 10 cysts of ME-49 type II *Toxoplasma gondii* (control group are Foxp3^{cre} mice without treatment) and subsequently followed for **g** body weight. **h** Mice were sacrificed 8 days after infection to assess colon length; **i** frequency of effector-like (CD44^{hi} CD62L^{lo}) conventional T lymphocytes in the indicated lymphoid organs; **j** frequency of IFN-γ producing CD4^{+} T cells after in vitro stimulation; **k** frequency of T-bet^{+} among Foxp3^{+}(Treg) cells. Data are representative of three independent experiments with n = 20 (**a, b**), n = 10-14 (**c, d**), n = 5 (**e**) or n = 10 (**g-k**) per group. Values are presented as the mean ± SD and were compared by two-tailed unpaired student's t-test (**a, c, g**), by Mantel-Cox test (**b**), by one-way ANOVA with Tukey's multiple comparisons test (**d, h**) or by two-way ANOVA with Tukey's multiple comparisons test (**i-k**). Only significant differences are indicated as follows: *: p<0.05, **: p<0.01, ***: p<0.001, ****: p<0.0001.

Figure 6. Concomitant loss of HIF2α but not HIF1α expression attenuates the proinflammatory phenotype of PHD2$^{\Delta Treg}$ mice.
a Representative gross autopsy of spleens and colon length summarized in **b** of Foxp3^{cre}, PHD2$^{\Delta Treg}$, PHD2-HIF1α$^{\Delta Treg}$, PHD2-HIF2α$^{\Delta Treg}$ and PHD2-HIF1α-HIF2α$^{\Delta Treg}$ (TKO) mice. **c** Representative merged (n = 15) t-distributed stochastic neighbor embedding (t-SNE) plot after dimensionality reduction and unsupervised clustering of flow cytometry data from CD4-expressing spleen cells. Relative distributions of CD4^{+} lymphocyte subsets are shown as doughnut charts. (**d-g**) Lymphoid cells from spleen, mesenteric (mLN), peripheral (pLN) lymph nodes or the small intestine lamina propria were collected from Foxp3^{cre}, PHD2$^{\Delta Treg}$, PHD2-HIF1α$^{\Delta Treg}$ mice, PHD2-HIF2α$^{\Delta Treg}$ and PHD2-HIF1α-HIF2α$^{\Delta Treg}$ (TKO) male and female mice and the relative frequency and phenotype of Foxp3-positive and Foxp3-negative, conventional T lymphocytes determined by flow cytometry. **d** Frequency of effector-like (CD44^{hi} CD62L^{lo}) conventional T lymphocytes in the indicated lymphoid organs. **e** Frequency of IFN-γ producing CD4^{+} T cells after in vitro stimulation. **f** Frequency of Foxp3-expressing cells among CD4-positive T lymphocytes. **g** Ratio of the Foxp3 MFI of PHD2-KO, PHD2-HIF1αKO, PHD2-HIF2αKO or TKO splenic Tregs to Foxp3^{cre} splenic Tregs. Data are representative of at least three independent experiments with n = 15 per groups. Values are expressed as the mean ± SD and were compared by One-way ANOVA with Tukey's multiple comparisons test (**b, g**) or by Two-way ANOVA with Tukey's multiple comparisons test (**d-f**). Only significant differences are indicated as follows: *: p<0.05, **: p<0.01, ***: p<0.001, ****: p<0.0001.

Figure 7. Anti-inflammatory response, response to chemokines and cell survival pathways represent targets of the PHD2-HIF2α axis in Tregs.
Splenic Treg cells were purified by cell sorting from Foxp3^{cre} (n = 3), PHD2$^{\Delta Treg}$ (n = 2), PHD2-HIF1α$^{\Delta Treg}$ (n = 2), PHD2-HIF2α$^{\Delta Treg}$ (n = 3) and PHD2-HIF1α-HIF2α$^{\Delta Treg}$ (TKO) (n = 3) male mice and total RNA was extracted and sequenced by RNA-sequencing (Illumina). **a** Heatmap of genes differentially expressed. Values are represented as Log_2 fold-change obtained from median of each gene and are plotted in red-blue color scale with red indicating increased expression and blue indicating decreased expression. Hierarchical clustering of genes (k mean clustering) show 20 clusters. **b** Classification of mouse strains according to their spontaneous inflammation severity. **c** Heatmap of genes downregulated when PHD2 and PHD2-HIF1α are deleted and whose expression is restored to a control level (close to Foxp3^{cre} Treg) following deletion of HIF2α (Cluster 10, 181 genes). **d** Heatmap of genes upregulated when PHD2 and PHD2-HIF1α are deleted and whose expression is restored to a control level following deletion of HIF2α (Cluster 11, 66 genes). **e** Heatmap of genes upregulated when PHD2 and PHD2-HIF2α are deleted and whose expression is restored to a control level following deletion of HIF1α (Cluster 3, 98 genes). Cluster 3, 10 and 11 were subjected to functional annotations and regulatory network analysis in the Ingenuity Pathway Analysis (IPA) software. Data were analyzed using Deseq2, a gene is differentially expressed when Log_2FC (Fold change) > 0.5 and FDR (False discovery rate) <0.05.

Figure 8. Identification of STAT1-mediated signaling as a target of the PHD2-HIF2α axis in Tregs.
a Upregulated and downregulated genes (cluster 10 and 11 in **Figure 6 c-d**) were imported into the Ingenuity Pathway Analysis (IPA) software and were subjected to Upstream regulator analysis (URA) prediction algorithms. STAT1 was predicted as an upstream regulators of downregulated genes with a p-value = 3.10^{-12}. Phosphorylated form of STAT1 (pSTAT1 (Tyr701)) was assessed by flow cytometry after brief in vitro stimulation (30 min) of splenic CD4$^+$ T lymphocytes with recombinant IFN-γ. **b** Representative histogram of pSTAT1 MFI for conventional CD4$^+$ T cells (Tconv) and Treg cells of Foxp3^{cre}, PHD2$^{\Delta Treg}$ and PHD2-HIF2α$^{\Delta Treg}$ male mice. Mean value expression (represented by MFI) of **c** pSTAT1 or **d** STAT1 total protein by splenic Treg of Foxp3^{cre}, PHD2$^{\Delta Treg}$ and PHD2-HIF2α$^{\Delta Treg}$ mice. **e** Frequency of Treg cells expressing the CXCR3 receptor. Data are representative of three independent experiments with n = 9 (**b-d**) or n = 12 (**e**) per groups. Values are presented as the mean ± SD and were compared by one-way ANOVA with Tukey's multiple comparisons. Only significant differences are indicated as follows: **: p<0.01,***: p<0.001.

Figure supplement legends

Figure 1-figure supplement 1. Treg-restricted loss of *Egln1* gene expression in PHD2$^{\Delta Treg}$ mice.
a Treg cells from Foxp3^{cre} male and female mice were purified by cell sorting from spleen (n = 10), mesenteric (mLN) (n = 8), peripheral (pLN) lymph nodes (n = 4) or the small intestine lamina propria (n = 4) and expression of *Egln2* (PHD1), *Egln1* (PHD2) and *Egln3* (PHD3) analyzed by qPCR. **b** YFP-positive (YFP^{+}) and YFP-negative (YFP^{-}) cells from PHD2-sufficient (Foxp3^{cre} mice) and PHD2-deficient (PHD2$^{\Delta Treg}$ mice) were purified by cell sorting from spleen and mesenteric lymph nodes (mLN) and expression of *Egln1* analyzed by qPCR. The graph demonstrates selective loss of *Egln1* gene expression in Tregs, but not in Tconvs purified from PHD2$^{\Delta Treg}$ mice. **c** *Ifng* gene expression relative to RPL32 by ex-vivo purified Tregs from spleen and mLN was determined by qPCR. **d** Representative flow cytometry expression profile of GLUT1, a specific HIF1α target gene in Foxp3 expressing or non-expressing cells from Foxp3^{cre} and PHD2$^{\Delta Treg}$ mice. **e** Frequency of GLUT1-expressing Tregs in lymphoid organs from Foxp3^{cre} and PHD2$^{\Delta Treg}$ mice. Data are representative of two independent experiments with n = 6 per group. Values are presented as the mean ± SD and were compared by two-tailed unpaired student's t-test. Only significant differences are indicated as follows: *: $p<0.05$, **: $p<0.01$, ***: $p<0.001$, ****: $p<0.0001$.

Figure 1-figure supplement 2. Increased blood cells counts and elevated hematocrit in PHD2$^{\Delta Treg}$ mice associated with an increase in vascular permeability.
a White blood cell (WBC) counts, **b** red blood cell (RBC) counts, **c** platelet (PLT) counts and **d** hematocrit (HCT) from Foxp3^{cre}, PHD2$^{\Delta Treg}$ and PHD2-HIF2α$^{\Delta Treg}$ male mouse blood. To assess vascular permeability mice were i.v injected with a 0,5% Blue Evans (BE) solution, and the indicated, organs collected after 30 minutes and placed in formamide at 55°C during 24 hours. The absorbance of supernatants was measured at 600 nm, **e** representative image of the colon supernatant after 24h in formamide, **f** ng of Blue Evans per mg of tissue for spleen, mesenteric lymph nodes (mLN), colon and liver of differents groups of mice injected or not with Blue Evans. Data are representative of two (a-d) or three (e-f) independent experiments with n = 7-9 per group (a-d) or n = 4-6 per group (e-f). Values are presented as the mean ± standard deviation (SD) and were compared by one-way ANOVA (**a-d**) or two-way ANOVA (**f**) with Tukey's multiple comparisons test. Only significant differences are indicated as follows: *: $p<0.05$, **: $p<0.01$, ***: $p<0.001$, ****: $p<0.0001$.

Figure 1-figure supplement 3. Gating strategy for flow cytometry data analysis.
Representative flow cytometry dot plots displaying the gating strategy for the identification of conventional T cell populations in Figures 1, 3, 4 and 5 and for identification of regulatory T cell subsets in Figures 2, 4 and 8

Figure 1-figure supplement 4. Absolute cell counts.
Absolute cell counts of **a** CD4^{+} T cells, **b** CD8^{+} T cells, **c** regulatory T cells and **d** activated conventional T cells in the spleen, mesenteric (mLN), peripheral (pLN) lymph

nodes and the small intestine lamina propria of Foxp3^{cre} and PHD2$^{\Delta Treg}$ male and female mice. Data are representative of at least three independent experiments with, n = 15 per group. Values are presented as the mean ± standard deviation (SD) and were compared by two-tailed unpaired student's t-test. Only significant differences are indicated as follows: *: p<0.05, **: p<0.01, ***: p<0.001, ****: p<0.0001.

Figure 5-figure supplement 1. PHD2$^{\Delta Treg}$ mice display a near-normal response to anti-CD3-induced enteritis.
Foxp3^{cre} and PHD2$^{\Delta Treg}$ female mice were injected twice i.p. with anti-CD3 mAbs (20µg) at two days interval and weighted daily. **a** Weight loss was found similar in both mouse strains tested; **b** relative expression of inflammatory mediators evaluated by qPCR on whole, unfractionated mesenteric lymph nodes. A similar, Th17-like response was observed in both mouse strains. Data are representative of two independent experiments with n = 6 per group. Values are presented as the mean ± SD and were compared by one-way ANOVA with Tukey's multiple comparisons test. Only significant differences are indicated as follows: *: p<0.05, **: p<0.01.

Figure 5-figure supplement 2. Loss of *Ifng* gene expression attenuates the pro-inflammatory phenotype of PHD2$^{\Delta Treg}$ mice
PHD2$^{\Delta Treg}$ mice were crossed with IFN-γKO mice (PHD2$^{\Delta Treg}$ IFN-γ^{KO} mice) and were compared to Foxp3^{cre} and PHD2$^{\Delta Treg}$ male and female mice and analyzed for **a** colon length; **b** frequency of effector-like (CD44^{hi} CD62L^{lo}) conventional T lymphocytes in the indicated lymphoid organs; **c** frequency of IFN-γ production after in vitro stimulation; **d** frequency of IL-17A-producing cells after in vitro stimulation and **e** frequency of Foxp3^{+} cells in the indicated lymphoid organs. Data are representative of three independent experiments with n = 10 per groups. Values are expressed as the mean ± SD and were compared by One-way ANOVA with Tukey's multiple comparisons test (**a**) or by Two-way ANOVA with Tukey's multiple comparisons test (**b-e**). Only significant differences are indicated as follows: *: p<0.05, **: p<0.01, ***: p<0.001, ****: p<0.0001.

Figure 6-figure supplement 1. Treg-selective HIF1α or HIF2α deficiency does not affect immune homeostasis in naive mice.
a Splenic Treg cells were purified by cell sorting from Foxp3^{cre} (n = 3), PHD2$^{\Delta Treg}$ (n = 2), PHD2-HIF1α$^{\Delta Treg}$ (n = 2), PHD2-HIF2α$^{\Delta Treg}$ (n = 3), PHD2-HIF1α-HIF2α$^{\Delta Treg}$ (TKO) (n = 3), HIF1α$^{\Delta Treg}$ (n = 3) and HIF2α$^{\Delta Treg}$ (n = 3) male mice and their genotype verified by qPCR on the extracted total RNA fraction. **b** representative gross autopsy findings revealing normal spleen and colon size (summarized in panel **c**) in 12 weeks aged male and female mice. **d** frequency of CD4^{+} Foxp3^{-} CD44^{hi} CD62L^{lo} cells in lymphoid organs; **e** frequency of CD4^{+} lymphocytes producing IFN-γ upon in vitro stimulation; **f** frequency of Foxp3^{+} cells in the indicated lymphoid organs; **g** Ratio of the Foxp3 MFI of HIF1αKO or HIF2αKO splenic Tregs to Foxp3^{cre} splenic Tregs. Data are representative of three independent experiments with n = 10. Values are presented as the mean ± SD and were compared by one-way ANOVA with Tukey's multiple comparisons test (**c, g**) or by Two-way ANOVA with Tukey's multiple comparisons test (**d-f**). No statistical difference were found between groups.

Figure 7-figure supplement 1. Signaling pathways affected by loss of PHD2-expression in Treg.
a Top significantly downregulated pathways in PHD2-deficient Tregs compared to Tregs from Foxp3^{cre} mice **b** top significantly upregulated pathways in PHD2-deficient Tregs compared to Tregs from Foxp3^{cre} mice. Affected pathways were determined by over representation analysis (ORA analysis) in R program after Deseq2 analysis. Dots color and size represent respectively FDR (false discovery rate) and the number of genes affected in a given pathway.

Figure 8-figure supplement 1. Gating strategy for identification of YFP^{+} cells.
Representative flow cytometry dot plots displaying the gating strategy for the identification of YFP positive populations in the: **a** spleen, **b** mLN, **c** thymus and **d** liver. Although the majority of YFP-expressing cells also expressed Foxp3, a minor population (from 1 to 3% depending on the organ considered) of YFP cells lacked expression of both CD45 and Foxp3, suggesting a possible expression of the Cre-recombinase in non-hematopoietic cells in PHD2$^{\Delta Treg}$ mice.

Source data files

Figure 1- source data 1
Figure 2- source data 1
Figure 3- source data 1
Figure 4- source data 1
Figure 5- source data 1
Figure 6- source data 1
Figure 7- source data 1
Figure 8- source data 1

Figure 1-figure supplement 1- source data 1
Figure 1-figure supplement 2- source data 1
Figure 1-figure supplement 4- source data 1
Figure 5-figure supplement 1- source data 1
Figure 5-figure supplement 2- source data 1
Figure 6-figure supplement 1- source data 1
Figure 7-figure supplement 1- source data 1

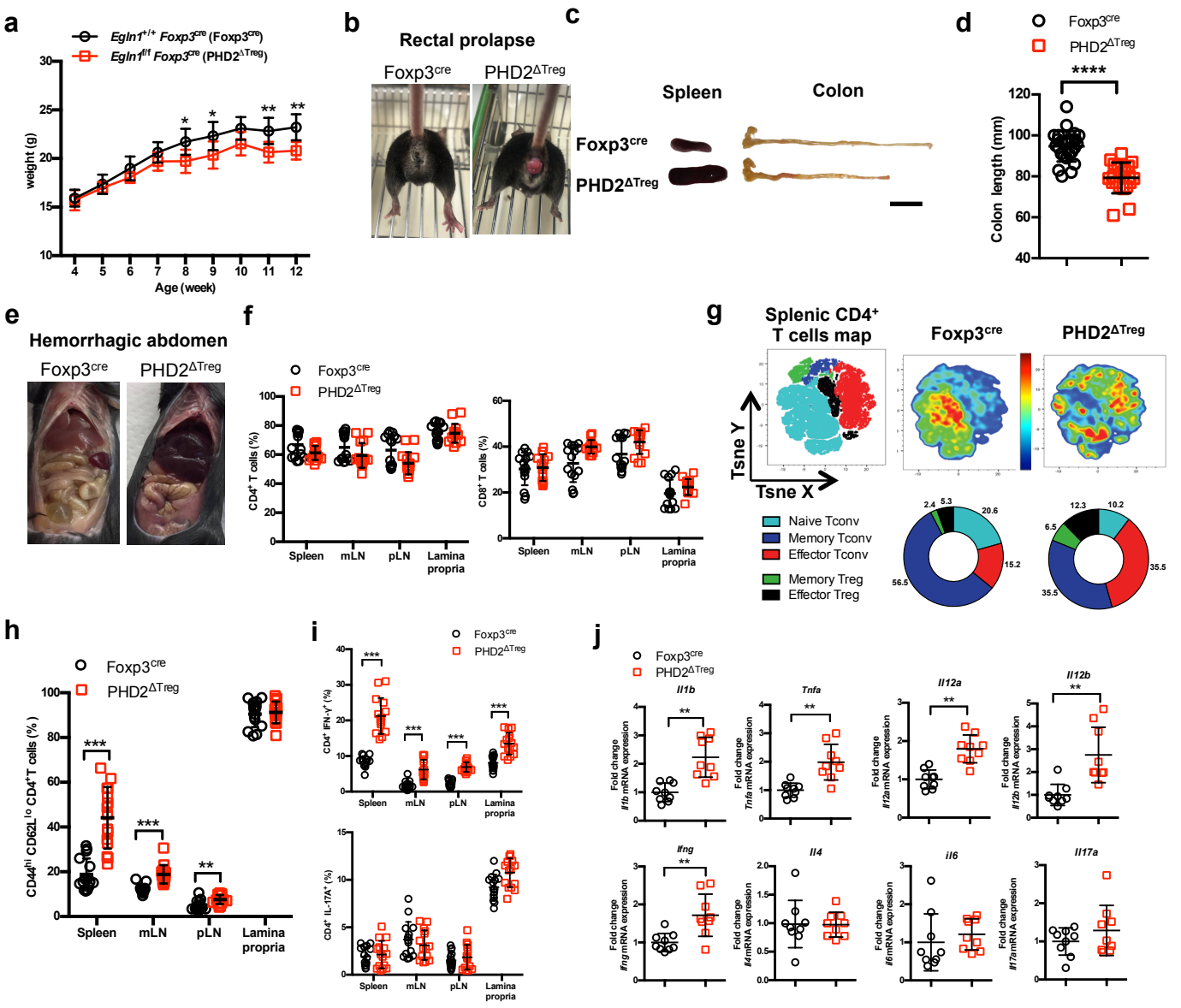

Figure 1. PHD2$^{\Delta Treg}$ mice display a spontaneous Th1-like inflammatory syndrome.

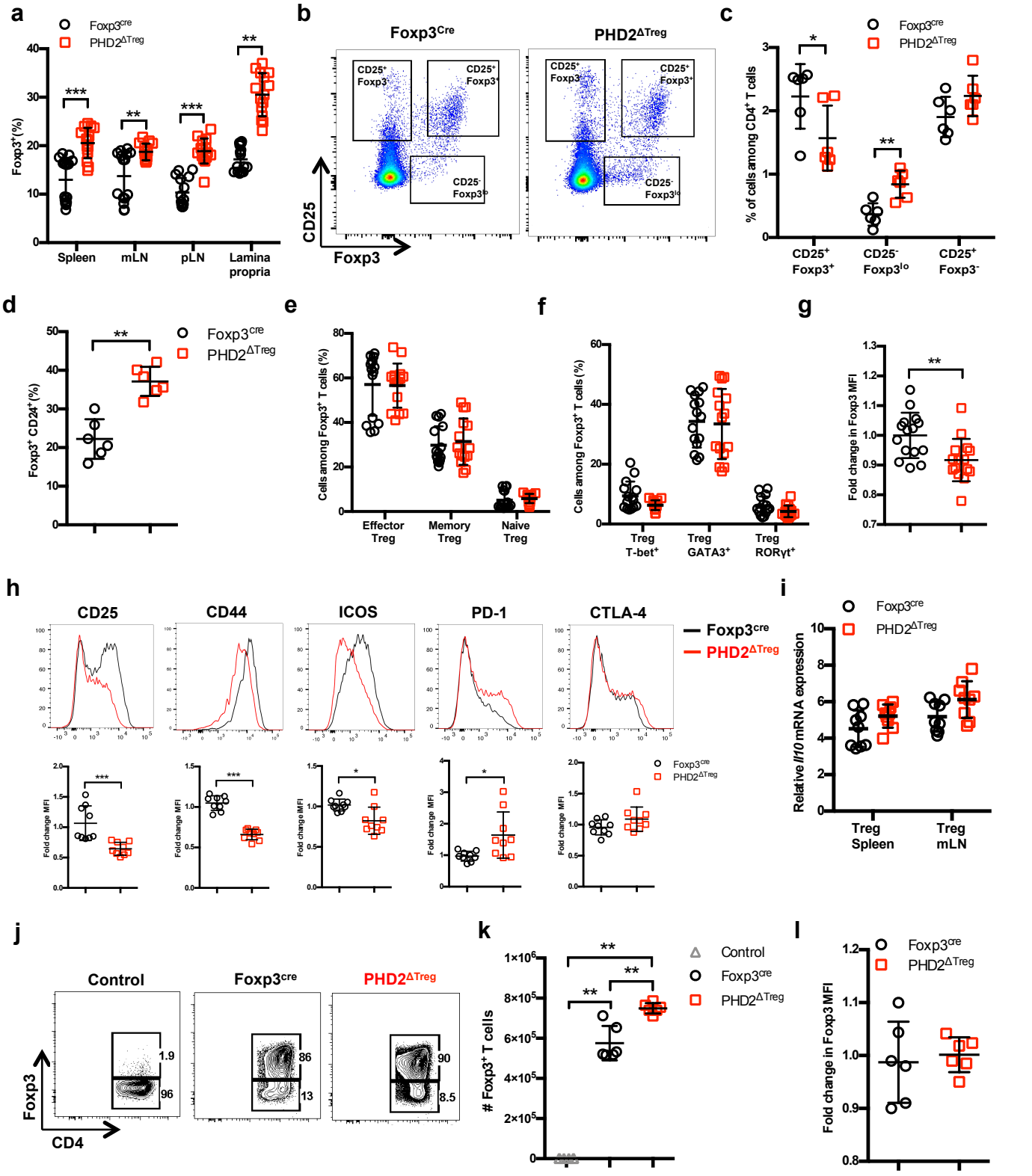

Figure 2. Increased number, but altered phenotype of PHD2-deficient Treg cells.

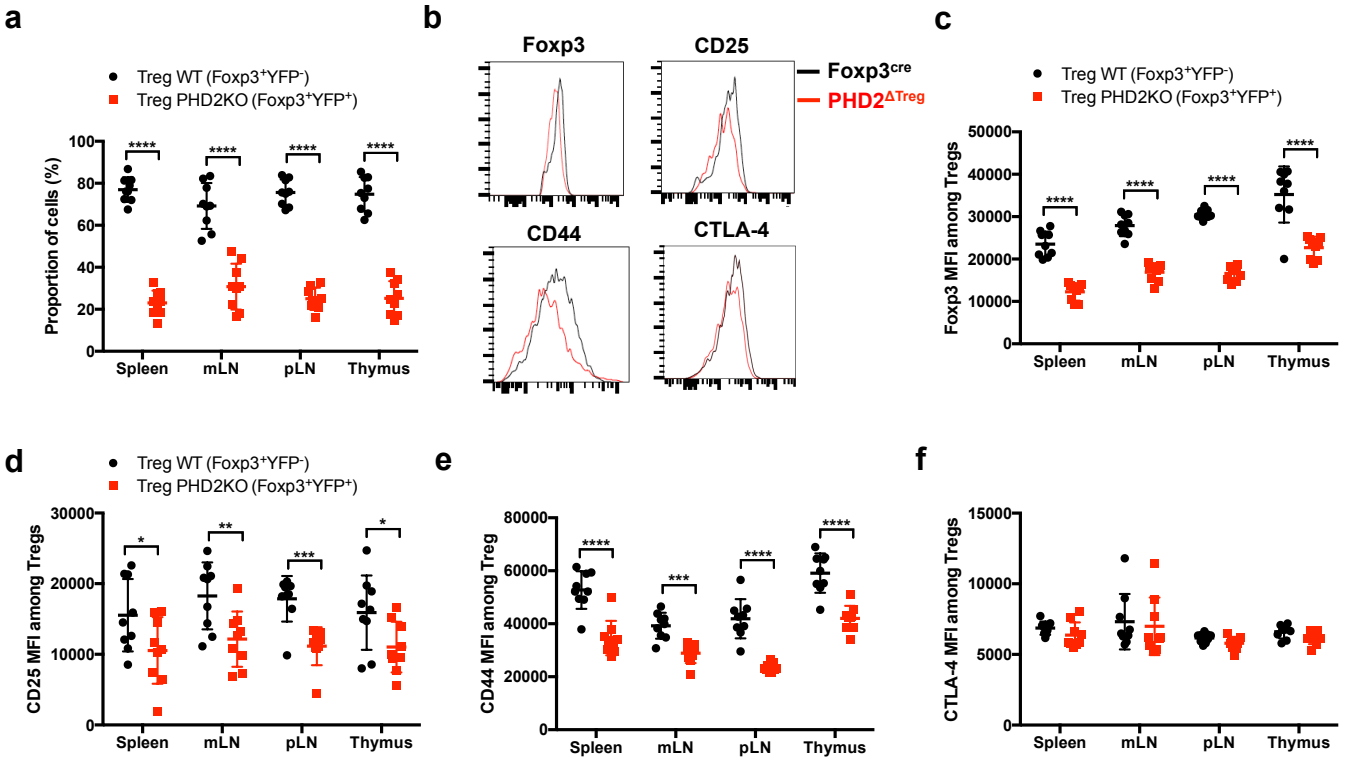

Figure 3. Cell autonomous role of PHD2 in determining Treg cells phenotype.

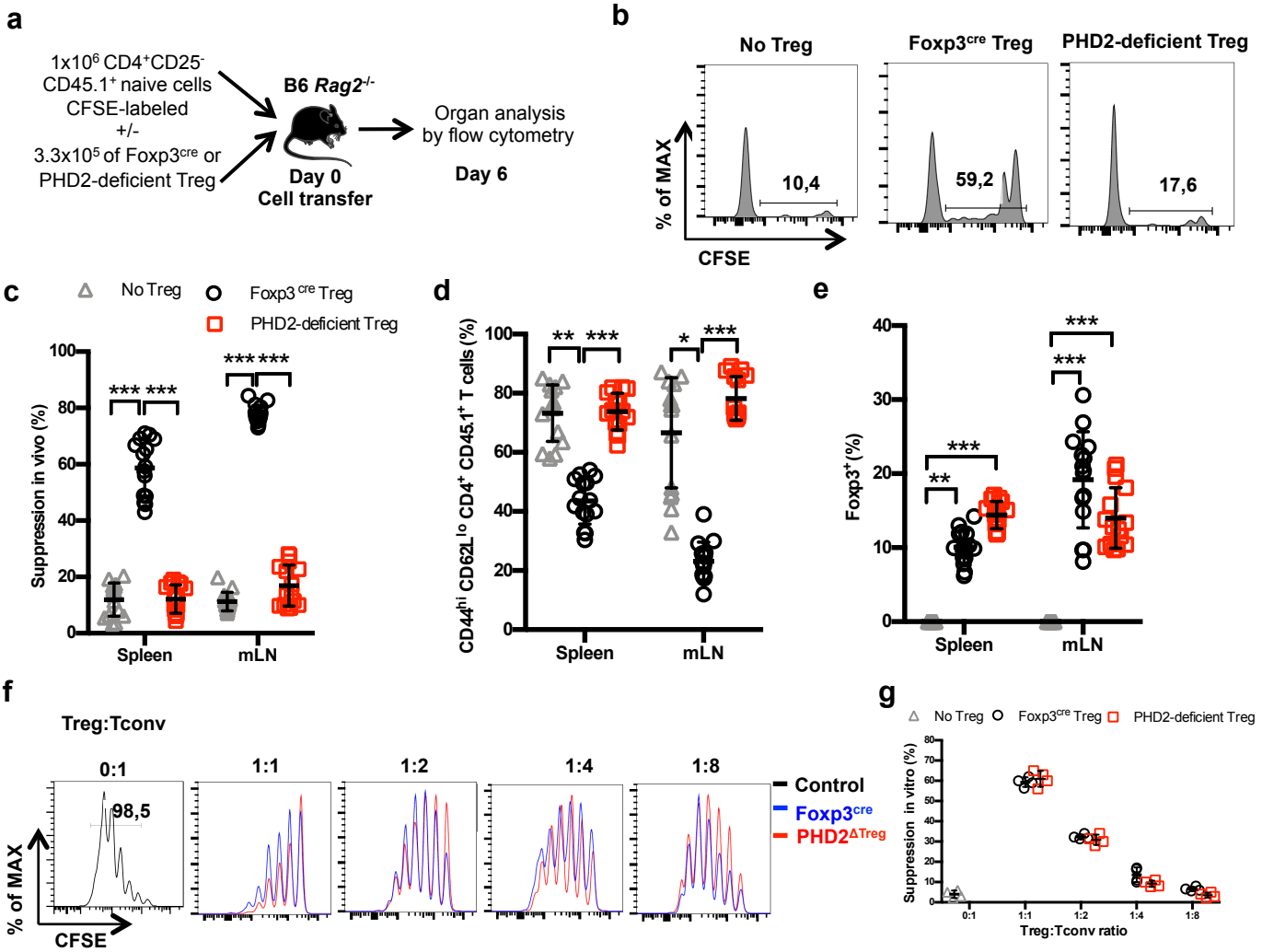

Figure 4. Reduced in vivo but not in vitro suppressive capacity of PHD2-deficient Treg.

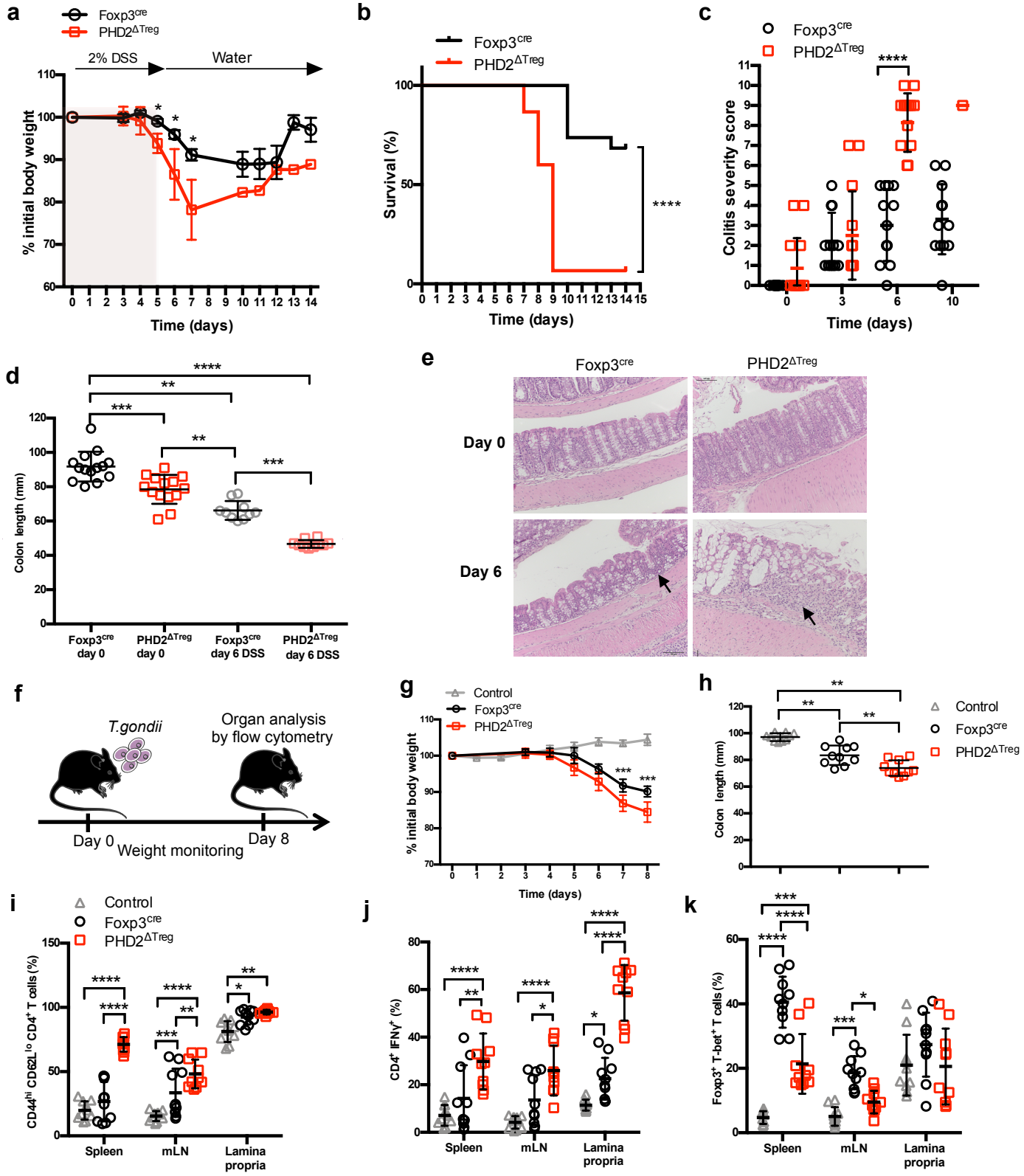

Figure 5. Increased sensitivity of PHD2$^{\Delta Treg}$ mice to DSS-induced colitis and toxoplasmosis.

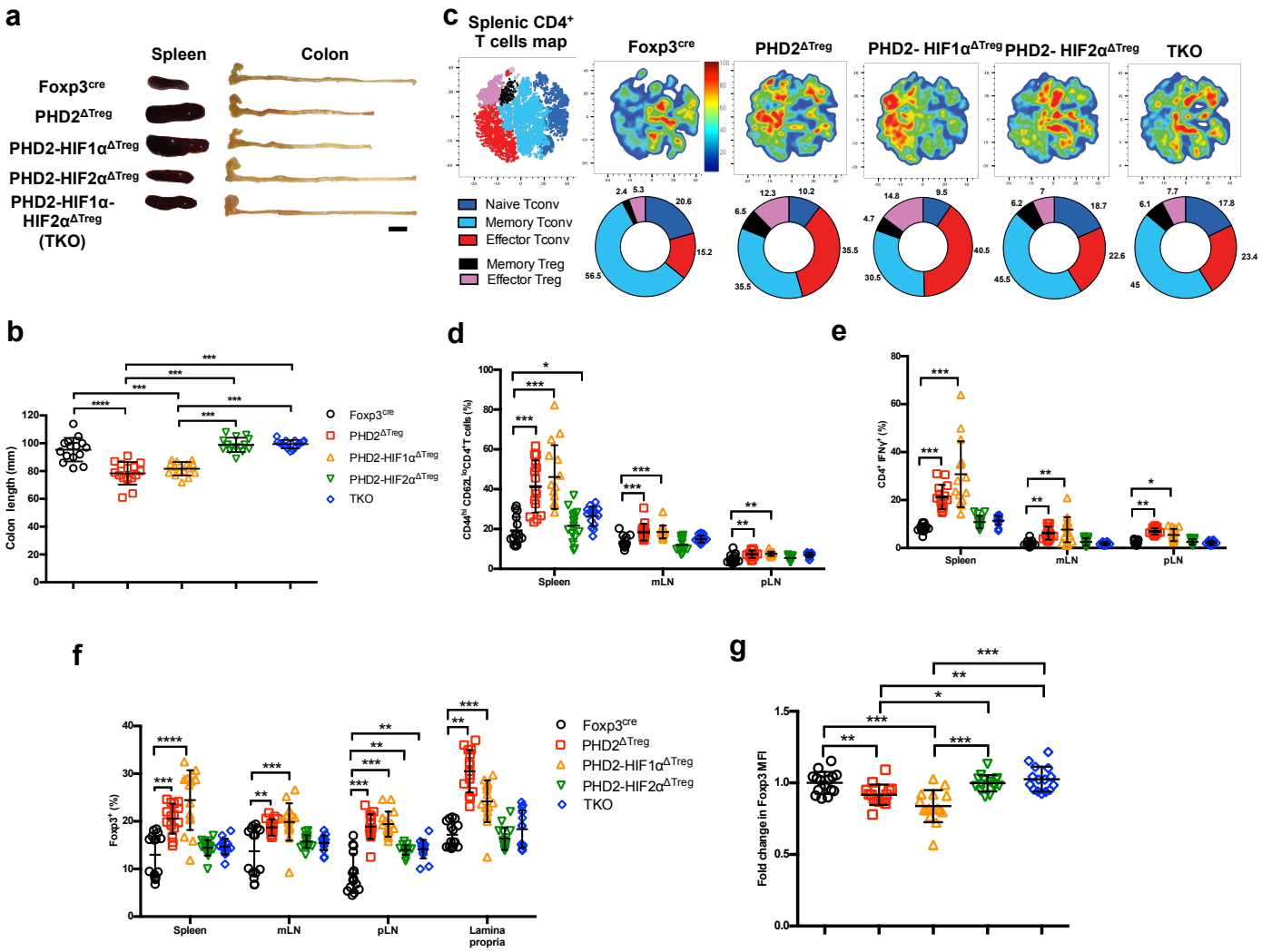

Figure 6. Concomitant loss of HIF2α but not HIF1α expression attenuates the proinflammatory phenotype of PHD2$^{\Delta Treg}$ mice.

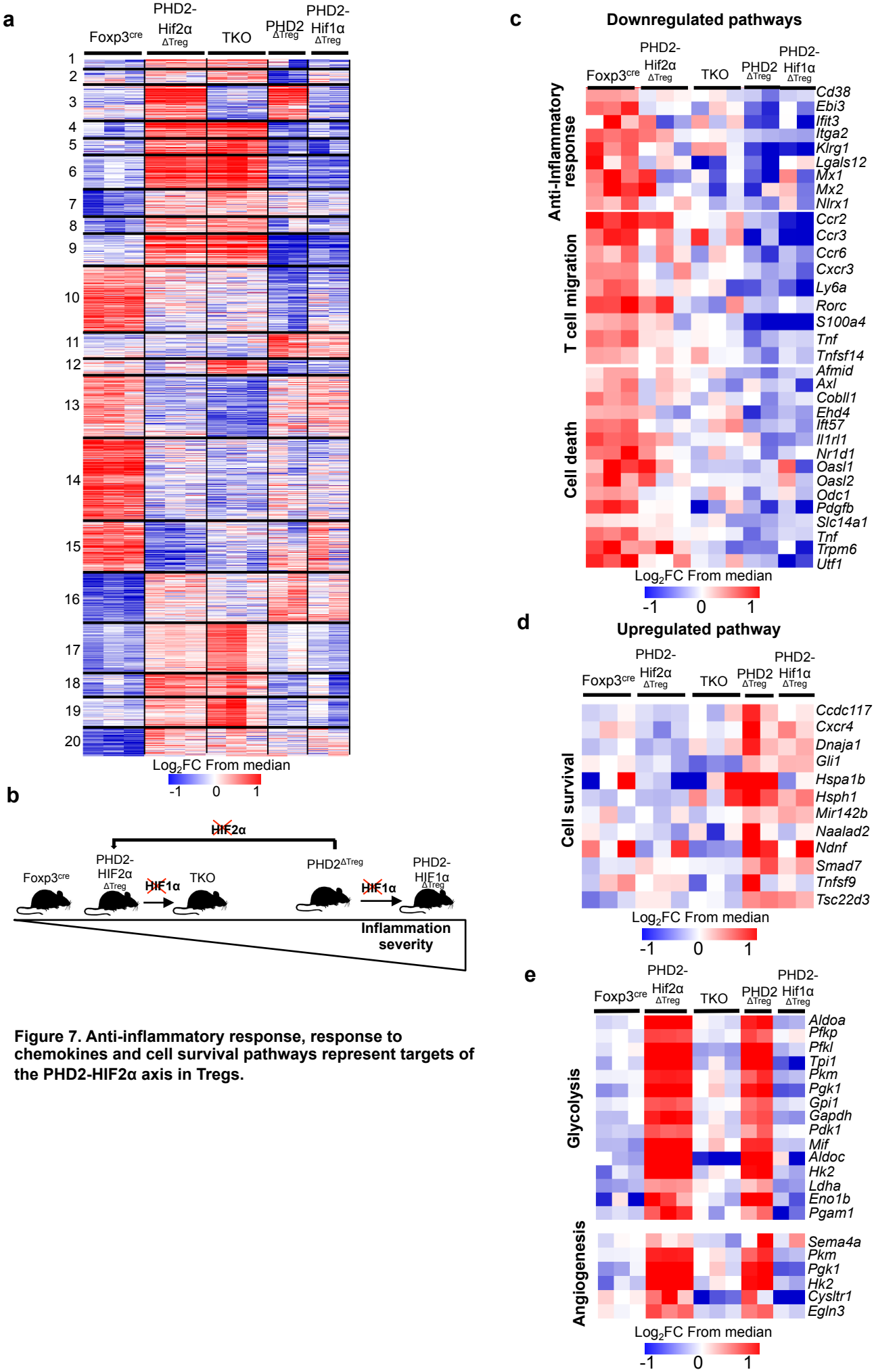

Figure 7. Anti-inflammatory response, response to chemokines and cell survival pathways represent targets of the PHD2-HIF2α axis in Tregs.

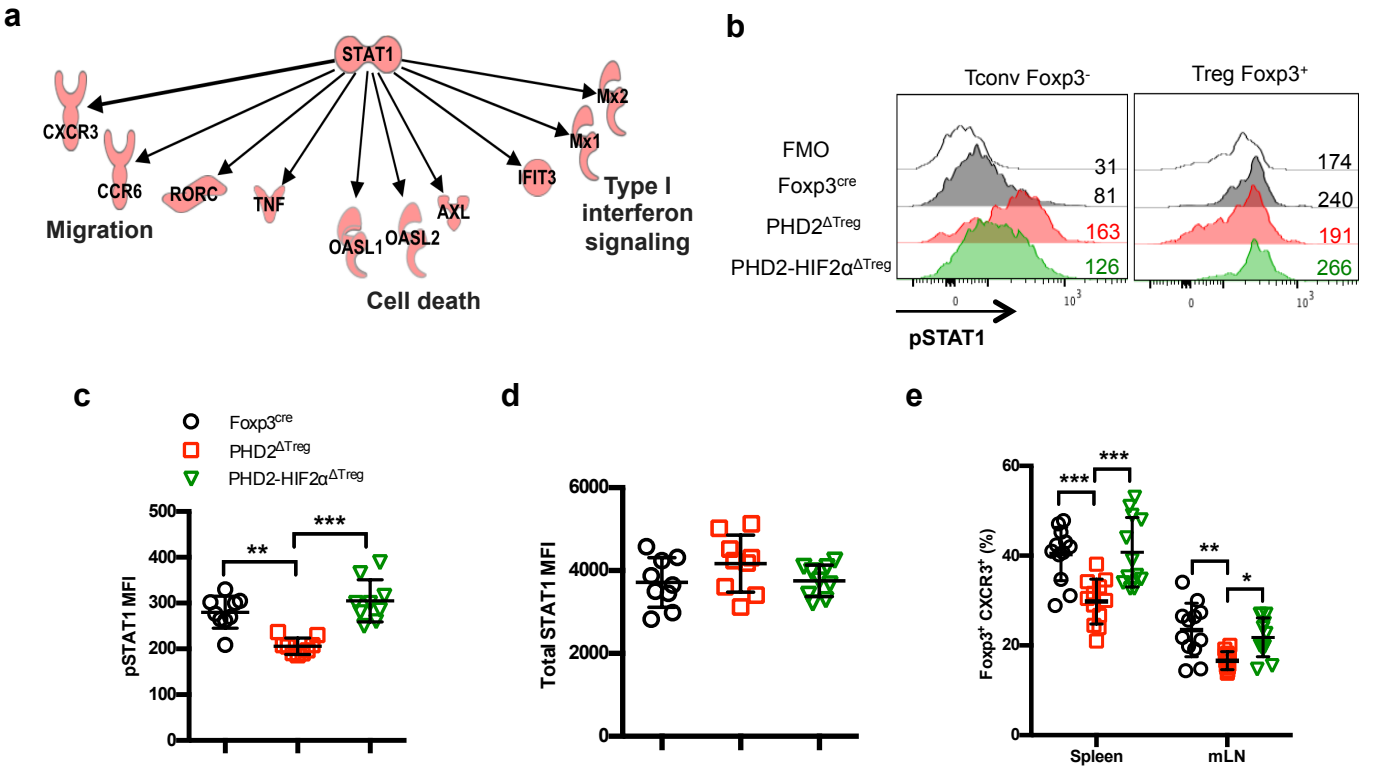

Figure 8. Identification of STAT1-mediated signaling as a target of the PHD2-HIF2α axis in Tregs.

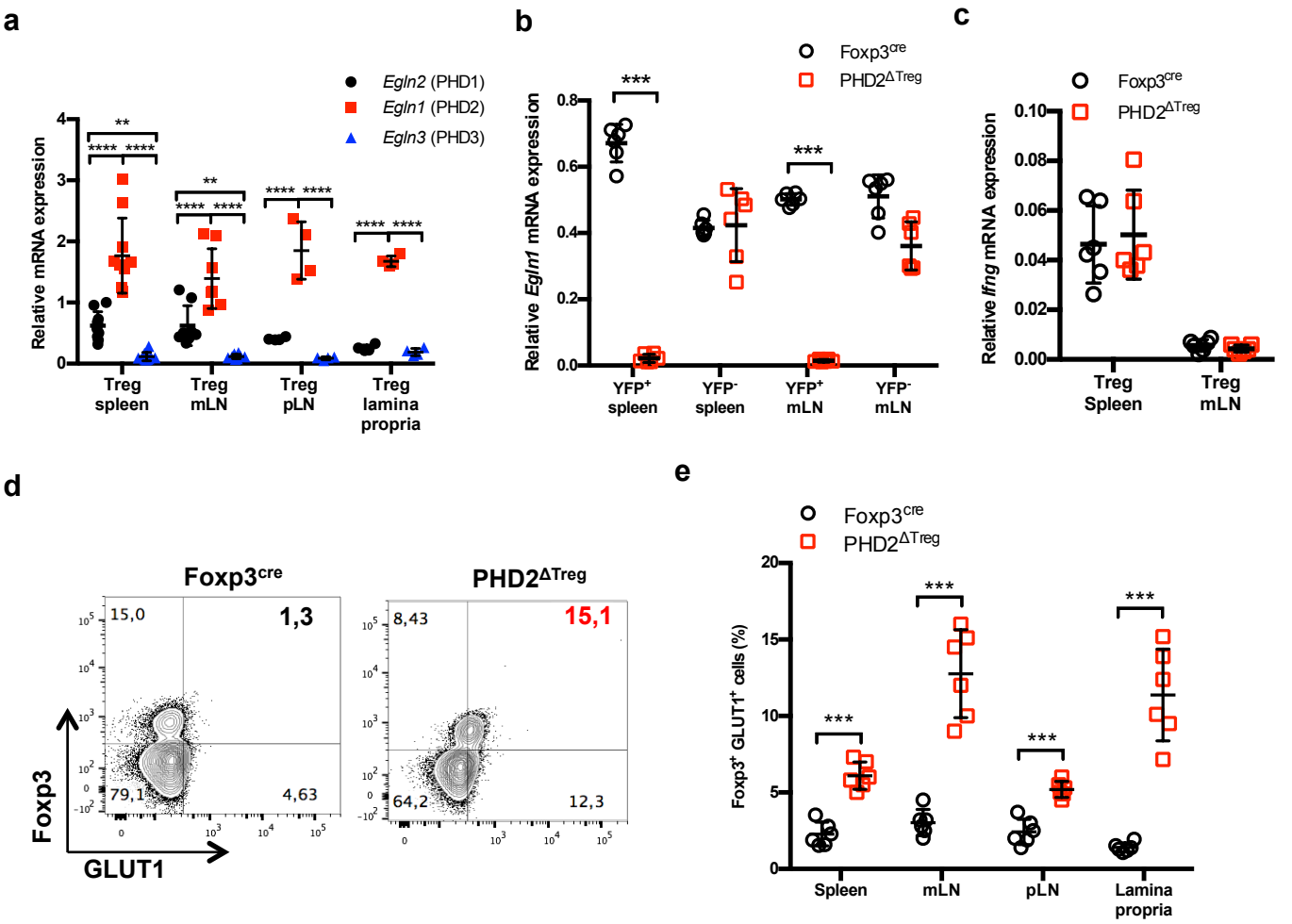

Figure 1-figure supplement 1. Treg-restricted loss of *Egln1* gene expression in PHD2$^{\Delta Treg}$ mice.

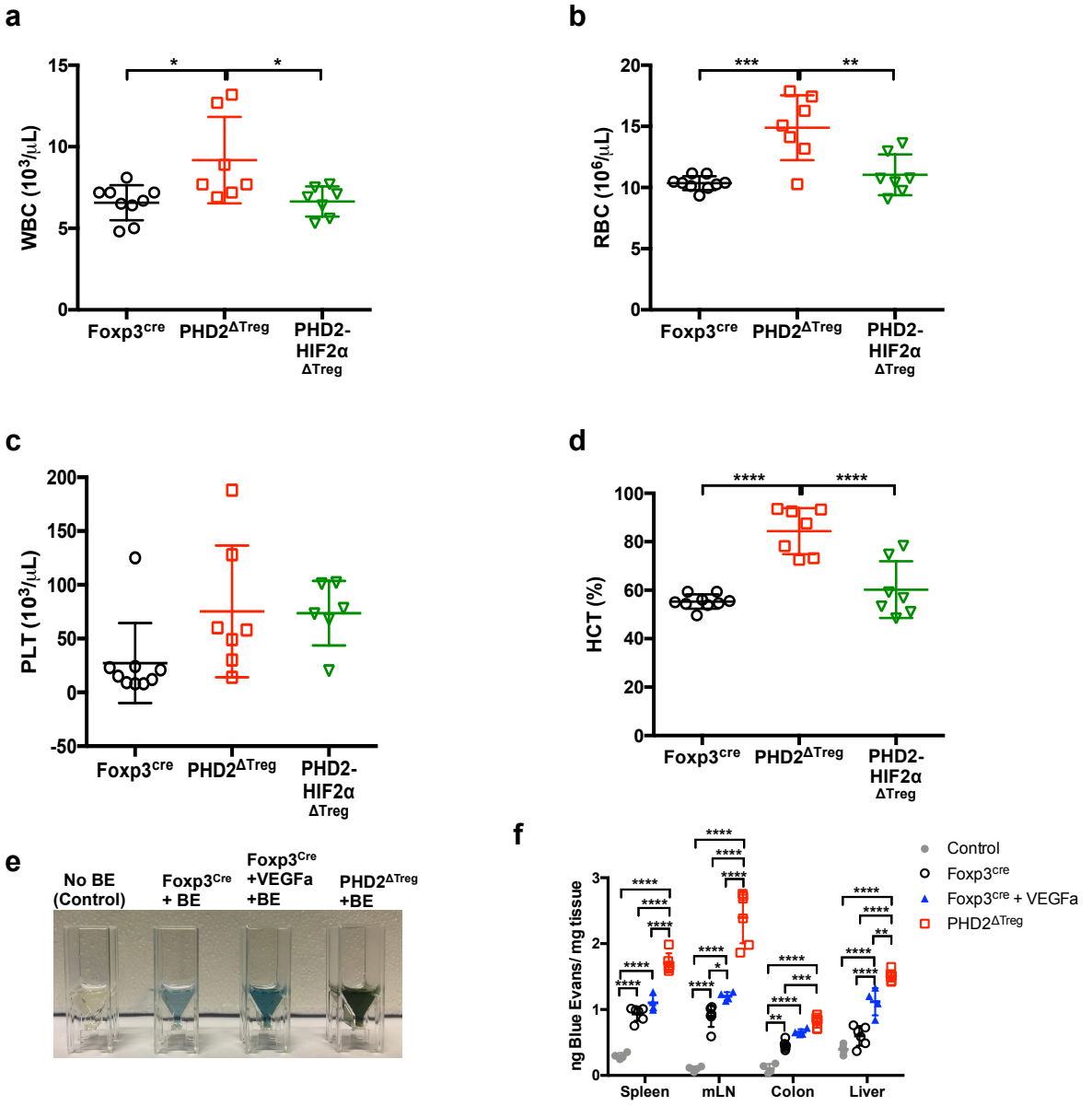

Figure 1-figure supplement 2. Increased blood cells counts and elevated hematocrit in PHD2$^{\Delta Treg}$ mice associated with an increase in vascular permeability.

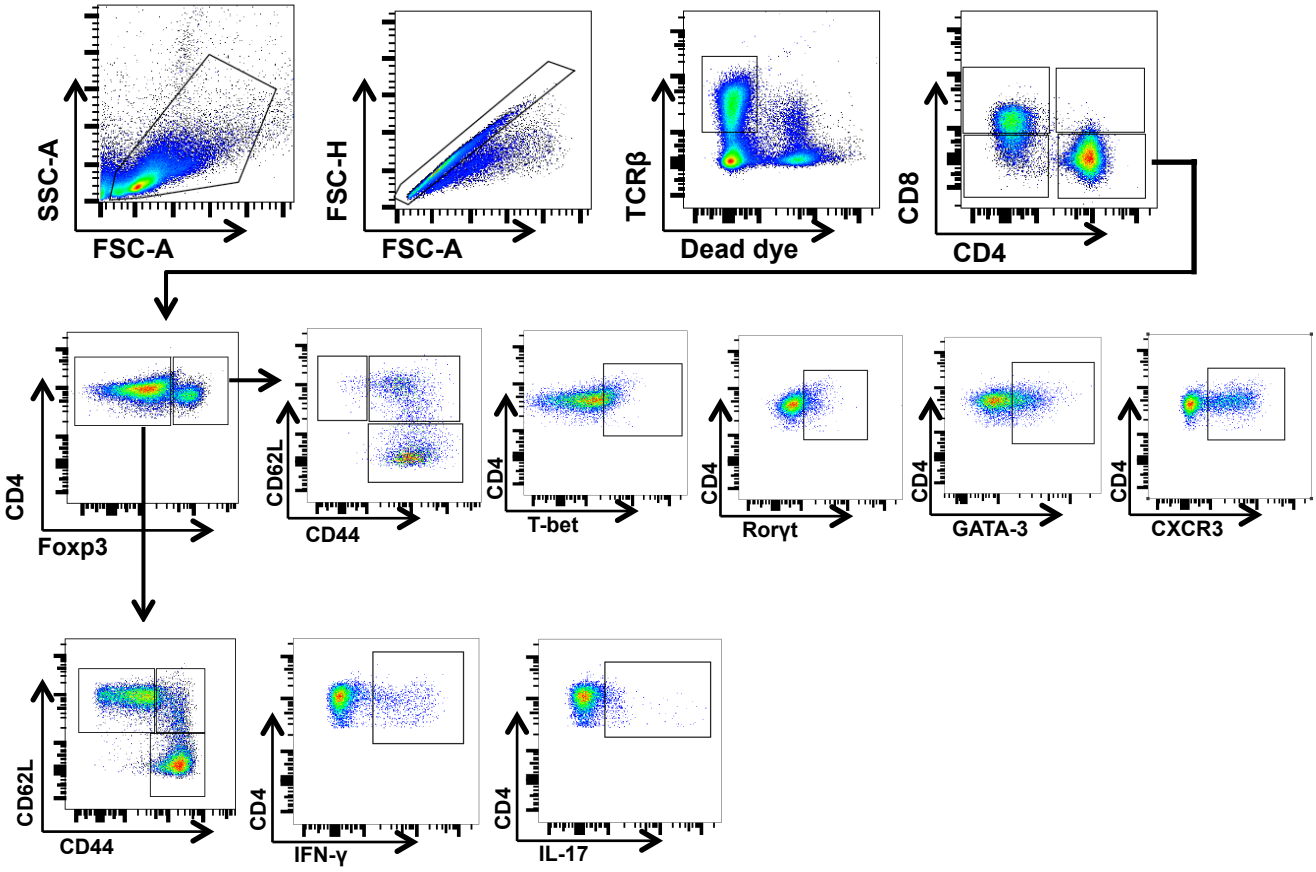

Figure 1-figure supplement 3. Gating strategy for flow cytometry data analysis.

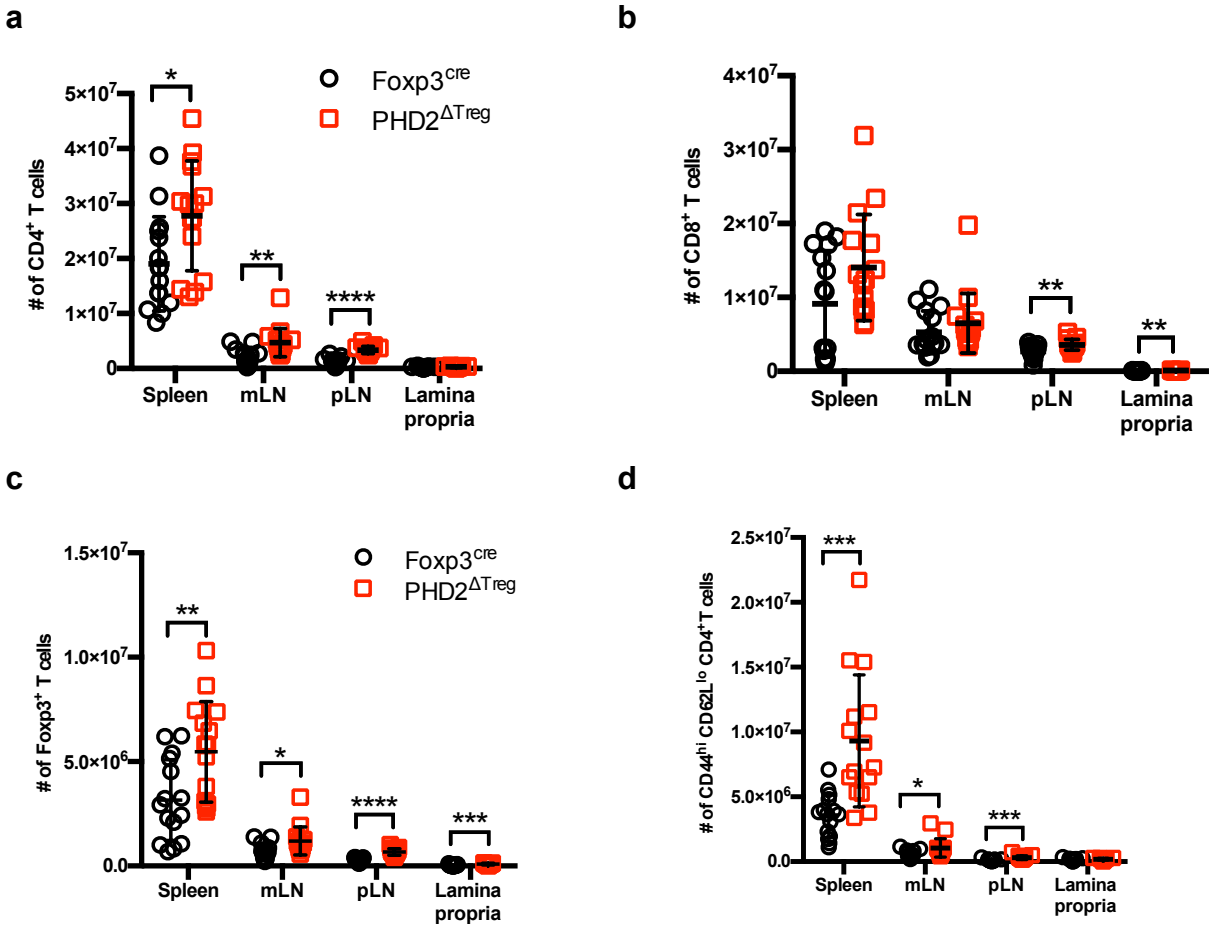

Figure 1-figure supplement 4. Absolute cell counts.

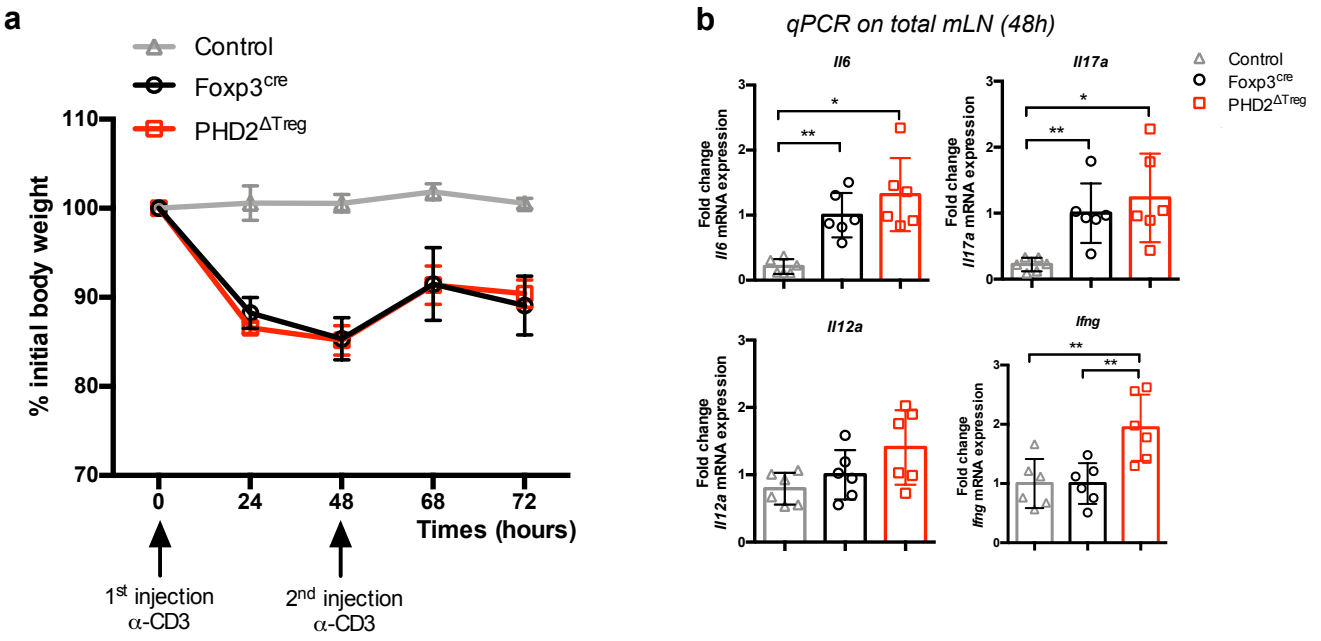

Figure 5-figure supplement 1. PHD2$^{\Delta Treg}$ mice display a near-normal response to anti-CD3-induced enteritis.

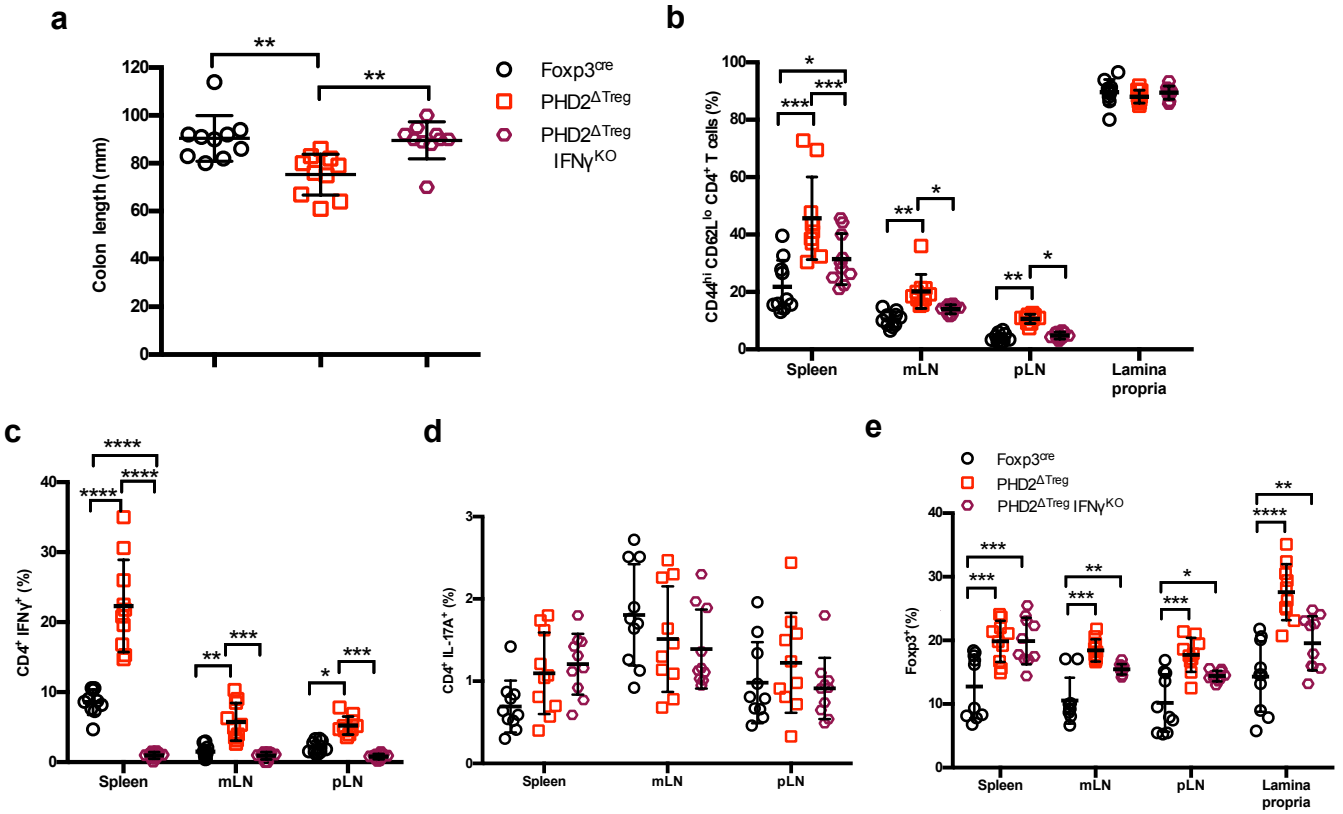

Figure 5-figure supplement 2. Loss of *Ifng* gene expression attenuates the pro-inflammatory phenotype of PHD2$^{\Delta Treg}$ mice

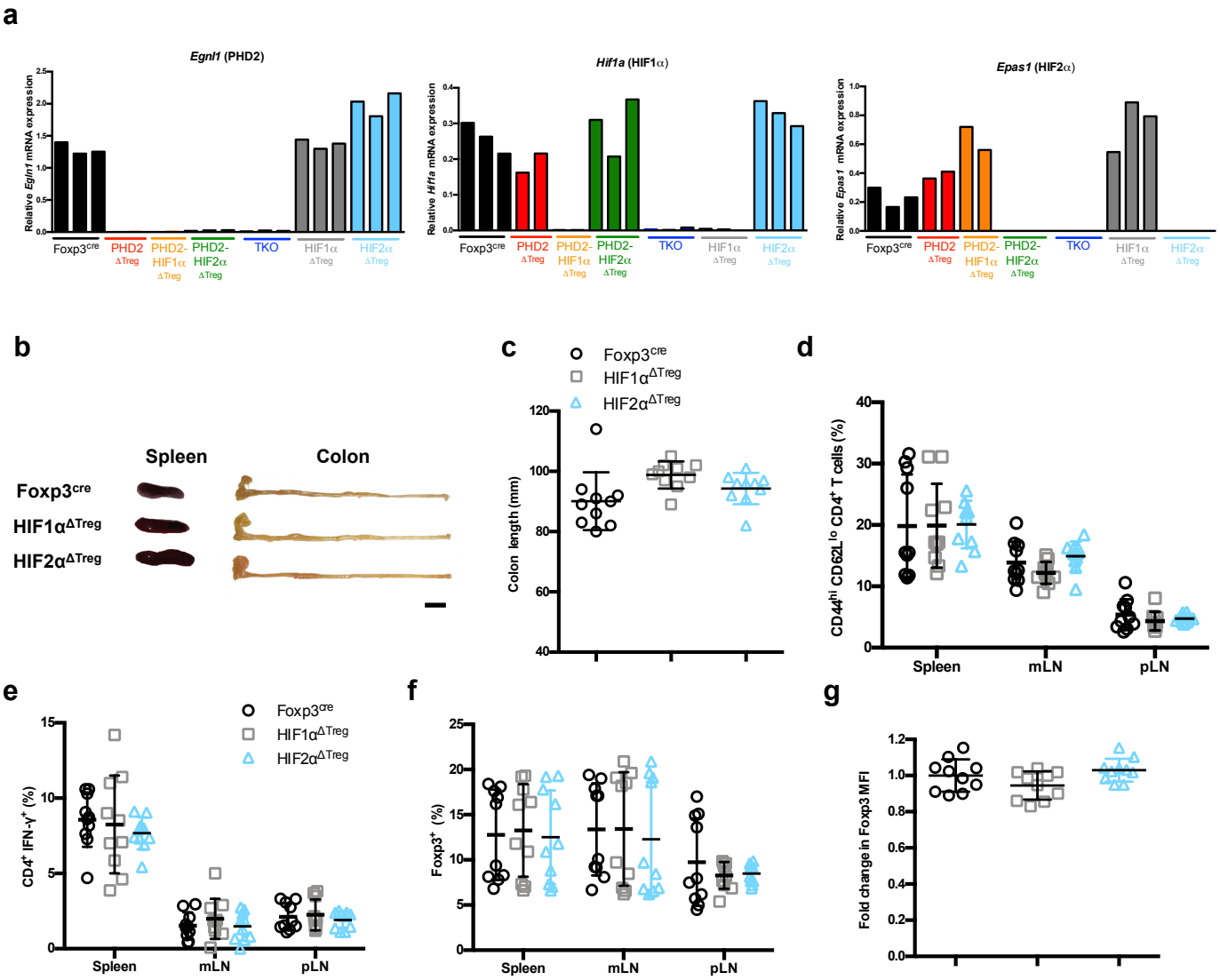

Figure 6-figure supplement 1. Treg-selective HIF1α or HIF2α deficiency does not affect immune homeostasis in naive mice.

a **Downregulated pathways**

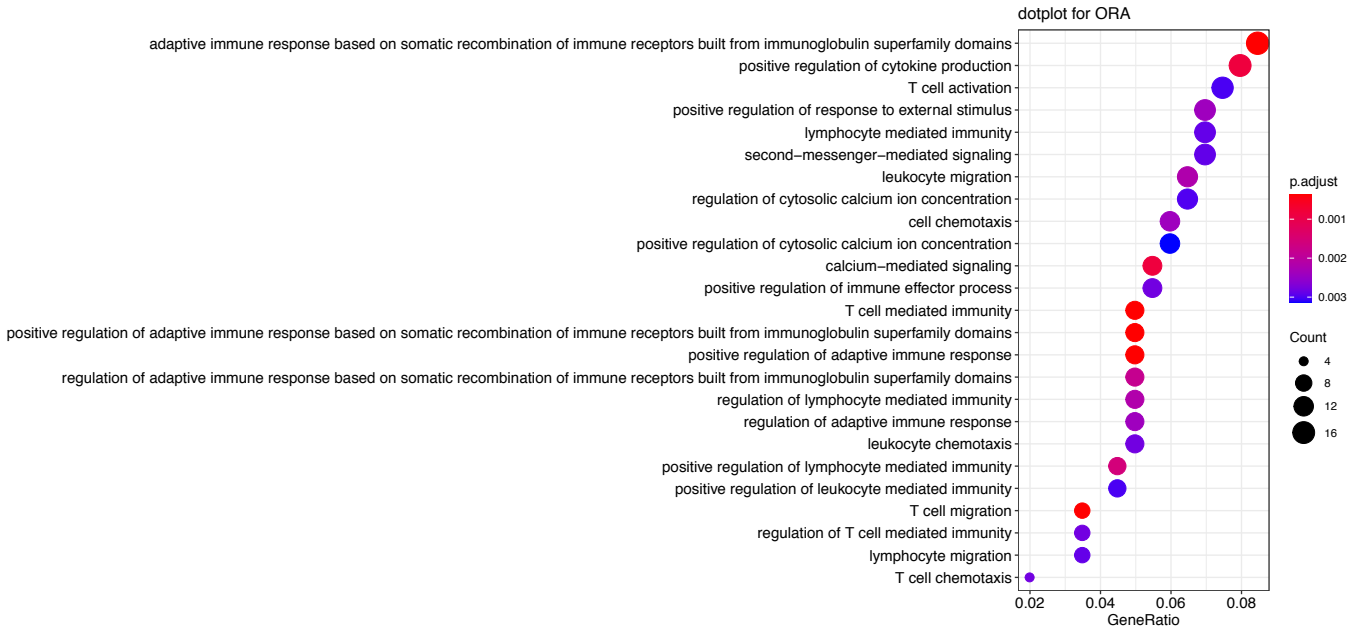

b **Upregulated pathways**

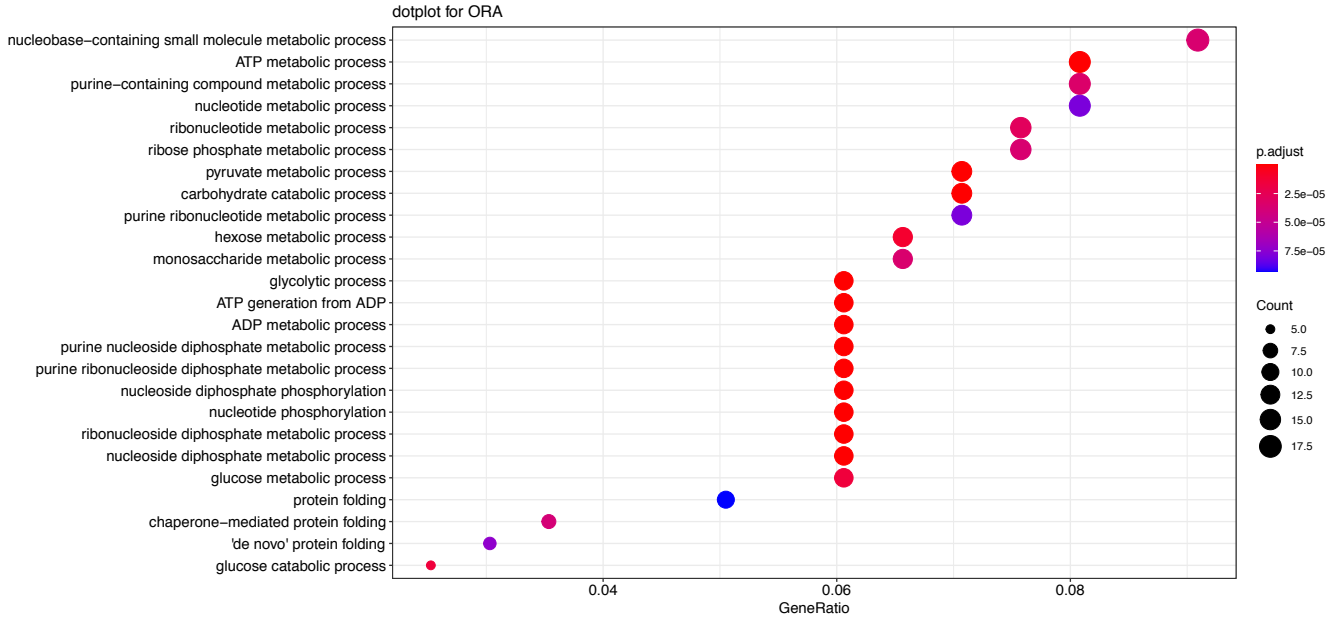

Figure 7-figure supplement 1. Signaling pathways affected by loss of PHD2-expression in Treg.

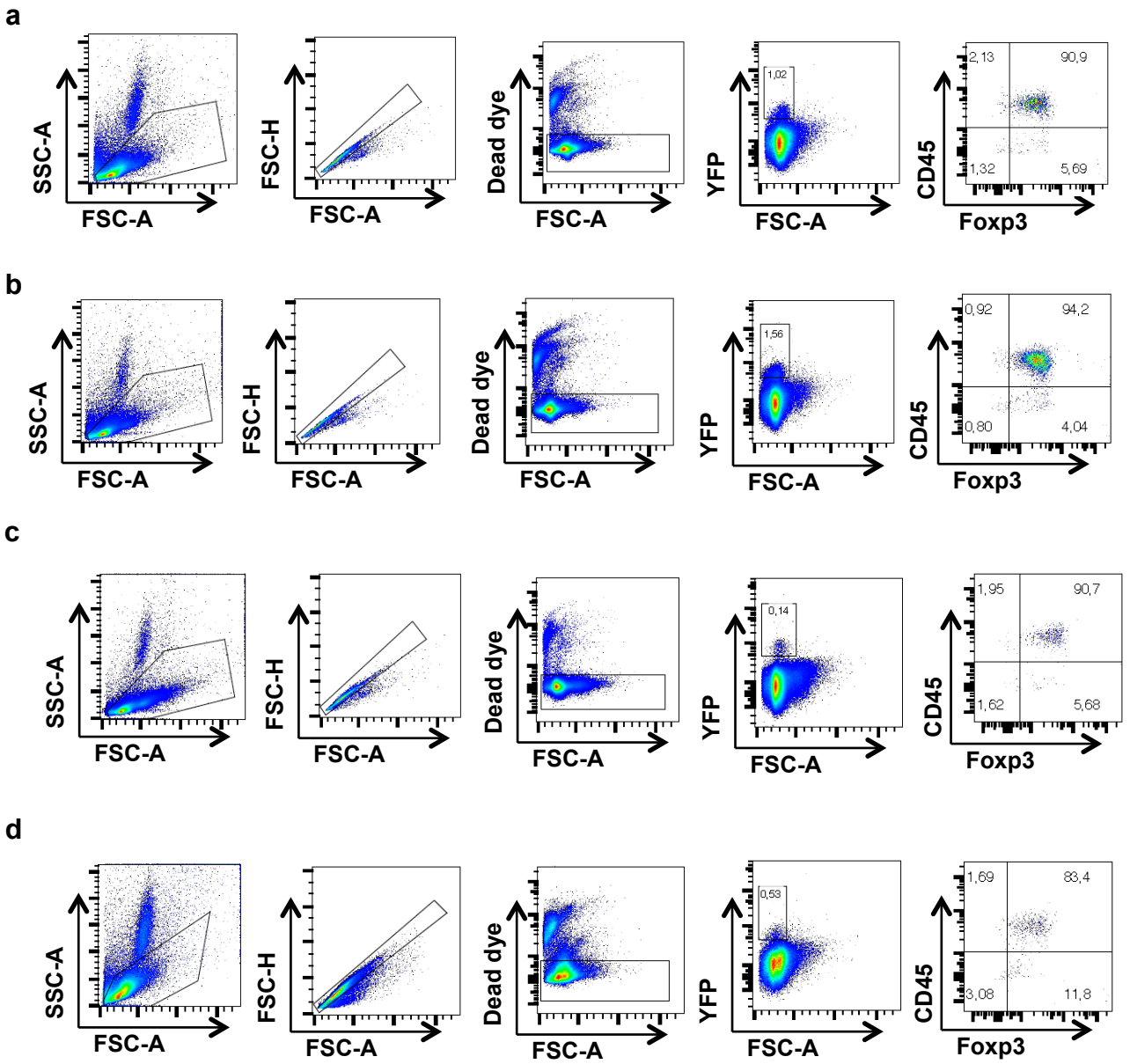

Figure 8-figure supplement 1. Gating strategy for identification of YFP^{+} cells.